Stony Brook University

Synthesis of Binary Nanocrystalline Aluminum Alloys

through High Energy Ball Milling

A Thesis Presented

by

Lacey L. Schwab

to

The Graduate School

in Partial Fulfillment of the

Requirements

for the Degree of

Master of Science

in

Materials Science & Engineering

Stony Brook University

May 2016

Stony Brook University

The Graduate School

Lacey L. Schwab

We, the thesis committee for the above candidate for the

Master of Science degree, hereby recommend

acceptance of this thesis.

Jason R. Trelewicz – Thesis Advisor
Assistant Professor, Department of Materials Science & Engineering

Sanjay Sampath – Second Reader
Distinguished Professor, Deparment of Materials Science & Engineering

This thesis is accepted by the Graduate School

Charles Taber
Dean of the Graduate School

Abstract of the Thesis

Synthesis of Binary Nanocrystalline Aluminum Alloys

through High Energy Ball Milling

by

Lacey L. Schwab

Master of Science

in

Materials Science & Engineering

Stony Brook University

2016

Nanocrystalline metals have useful mechanical properties such as high strength, improved wear resistance, and longer fatigue life; however, they are relatively unstable – grain boundary doping is a viable method towards stabilization [1-3]. After comparing the work of Murdoch and Schuh, that used a thermodynamic model to estimate grain boundary segregation enthalpy to the experimental work of Umbrajkar et al., it was realized that mechanical alloying is a processing route for grain boundary stabilization [10,11]. Whether or not chemical mixing has occurred is a good indicator of a powder system's potential for grain boundary doping. 99Al1Si, 99Al1Mg, 99Al1Zr, and 99Al11Zn were mechanically alloyed with a Retch 100 Planetary Bal Mill. The samples were then analyzed with a Rigaku Ultima III X-ray Diffractometer to determine whether or not these powder systems have chemically mixed. It was found that the 99Al1Mg powder system chemically mixed during the 8Hr, 8mL run and during the 16Hr, 16.5mL run, and the 99Al1Zr powder system chemically mixed during the 4Hr, 16.5mL run. The enthalpy of segregation values for each binary powder system correlated to the degree of mixing shown in these results.

Dedication Page

This thesis is dedicated to my grandparents, Leon and Carolyn Bruckner, who are two of the most incredible people I have ever met. I am eternally grateful and appreciative that two such wonderful people have played a large role in making me who I am today. I certainly would not be the person, or the engineer, that I am without their unconditional love, guidance, and support throughout my education. They make me feel extremely lucky to be their granddaughter. Thank you both for everything.

Table of Contents

Chapter I: Introduction……....1

1.1. Materials Science Fundamentals……...4

1.1.1. Hardness…….....4

1.1.2. Severe Plastic Deformation……...5

1.1.3. Cold Welding……..... 5

1.1.4. Fracturing…….. 6

1.2. Synthesis – Mechanical Alloying (MA)……... 6

1.2.1. Mechanical Alloying Variables…….....7

1.2.1.1. Type of Mill……...8

1.2.1.2. Milling Speed…….....8

1.2.1.3. Milling Container……...9

1.2.1.4. Milling Time……..9

1.2.1.5. Size and Type of Grinding Medium……..... 10

1.2.1.6. Percent of Empty Space in Jar…….....11

1.2.1.7. Milling Atmosphere…….....12

1.2.1.8. Ball-to-Powder Ratio (BPR)…….....12

1.2.1.9. Process Control Agent (PCA)……..13

1.2.10. Temperature of Milling…….....15

1.3. Mechanism of Alloying – High Energy Milling…….....18

1.3.1. Ductile-Ductile MA Systems…….. 22

1.3.2. Ductile-Brittle MA Systems……..…..24

1.3.3. Planetary Ball Mill……..26

1.4. Problem Statement……..28

Table of Contents

Chapter 2: Materials and Methods……..…….....30

2.1. Materials – Binary Systems……....….30

2.2. Characterization – X-ray Diffraction……. …..31

2.2.1. X-ray Diffraction Instrumentation – Rigaku Ultima III…..……..... ….32

2.2.2. X-ray Powder Diffraction Fundamentals……...…..34

2.2.3. XRD Data Analysis – Jade…….…….....38

2.3. Experimental Procedure and Chosen Parameters……...…….....39

2.3.1. General Ball Milling Procedure…….……...39

2.3.2. Ball Milling – Chosen Parameters…….....42

2.3.3. General X-ray Diffraction Procedure……... 43

2.3.4. X-ray Diffraction – Chosen Parameters…….... 46

Chapter 3: Results and Discussion…… 48

3.1. Aluminum-Silicon Alloys……..…….. 48

3.2. Aluminum-Zinc Alloys……..…….. 52

3.3. Aluminum-Magnesium Alloys……..……...56

3.4. Aluminum-Zirconium Alloys……..…….....61

3.5. Synthesis of Results…… 65

Chapter 4: Concluding Remarks and Future Work…….....74

References…….....78

List of Figures/Tables/Illustrations

Figure 1: Non-equilibrium synthesis used in mechanical alloying (page 5)

Figure 2: Milling time required for amorphization versus normalized milling temperature (page 17)

Figure 3: Collisions between ball and powders during mechanical alloying (page 18)

Figure 4: Average particle size and milling time relationship (page 20)

Figure 5: Logarithmic relationship between milling time versus particle size (page 22)

Figure 6: Convoluted lamellar layer of ductile-ductile component system (page 23)

Figure 7: Deformation characteristics of starting powders used during mechanical alloying (page 24)

Figure 8: Structural evolution during mechanical alloying of ductile-brittle powder systems (page 25)

Figure 9: TEM image of a brittle component which is incompatible with a ductile component (page 26)

Figure 10: Retsch PM100 Planetary Ball Mill (page 27)

Figure 11: Schematic of planetary ball mill in motion (page 28)

Figure 12: Rigaku Ultima III X-ray Diffractometer (page 32)

Figure 13: X-ray tube, sample holder, and X-ray detector within Ultima III (page 33)

Figure 14: Schematic representation of Bragg's Law (page 35)

Figure 15: Instrumental effects on peak broadening (page 35)

Figure 16: Williamson-Hall plot to derive crystal size and strain (page 37)

Figure 17: Peak Profile Fitting program output in Jade (page 38)

Figure 18: Powder sample holder (page 43)

Figure 19: Divergence height limiting slit (page 44)

Figure 20: Schematic of the goniometer's layout (page 44)

Figure 21: S-curve generated by initial Z scan (page 45)

List of Figures/Tables/Illustrations

Figure 22: XRD data for unmilled aluminum powder (page 48)

Figure 23: XRD data for 99Al1Si, 1Hr Run, 16.5mL (page 49)

Figure 24: XRD data for 99Al1Si, 4Hr Run, 16.5mL (page 49)

Figure 25: XRD data for 99Al1Si, 8Hr Run, 16.5mL (page 50)

Figure 26: XRD data for 99Al1Si, 16Hr Run, 16.5mL (page 50)

Figure 27: XRD data for 99Al1Si, 8Hr Run, 8mL (page 51)

Figure 28: XRD data for 99Al1Si, 8Hr Run, Volume Comparison (page 51)

Figure 29: XRD data for 99Al1Si, Milling Time Comparison, 16.5mL (page 52)

Figure 30: XRD data for 99Al1Zn, 1Hr Run, 16.5mL (page 53)

Figure 31: XRD data for 99Al1Zn, 4Hr Run, 16.5mL (page 53)

Figure 32: XRD data for 99Al1Zn, 8Hr Run, 16.5mL (page 54)

Figure 33: XRD data for 99Al1Zn, 8Hr Run, 8mL (page 54)

Figure 34: XRD data for 99Al1Zn, 8Hr Run, Volume Comparison (page 55)

Figure 35: XRD data for 99Al1Zn, Milling Time Comparison, 16.5mL (page 55)

Figure 36: XRD data for 99Al1Mg, 1Hr Run, 8mL (page 56)

Figure 37: XRD data for 99Al1Mg, 4Hr Run, 8mL (page 57)

Figure 38: XRD data for 99Al1Mg, 8Hr Run, 8mL (page 57)

Figure 39: XRD data for 99Al1Mg, Time Milling Comparison, 8mL (page 58)

Figure 40: XRD data for 99Al1Mg, 1Hr Run, 16.5mL (page 58)

Figure 41: XRD data for 99Al1Mg, 4Hr Run, 16.5mL (page 59)

Figure 42: XRD data for 99Al1Mg, 8Hr Run, 16.5mL (page 59)

Figure 43: XRD data for 99Al1Mg, 16Hr Run, 16.5mL (page 60)

Figure 44: XRD data for 99Al1Mg, 8Hr Run, Volume Comparison (page 60)

List of Figures/Tables/Illustrations

Figure 45: XRD data for 99Al1Mg, Milling Time Comparison, 16.5mL (page 61)

Figure 46: XRD data for 99Al1Zr, 1Hr Run, 16.5mL (page 62)

Figure 47: XRD data for 99Al1Zr, 4Hr Run, 16.5mL (page 62)

Figure 48: XRD data for 99Al1Zr, 8Hr Run, 16.5mL (page 63)

Figure 49: XRD data for 99Al1Zr, 8Hr Run, 8mL (page 63)

Figure 50: XRD data for 99Al1Zr, 16Hr Run, 16.5mL (page 64)

Figure 51: XRD data for 99Al1Zr, 8Hr Run, Volume Comparison (page 64)

Figure 52: XRD data for 99Al1Zr, Milling Time Comparison, 16.5mL (page 65)

Figure 53: Grain size v. milling time for tungsten alloys (page 69)

Figure 54(a): Grain size v. milling time for aluminum alloys (page 70)

Figure 54(b): Grain size exponential refinement trend v. milling time for aluminum alloys (page 70)

Figure 55: Table of solute v. solvent and range of values for enthalpy of segregation (page 72)

Table 1: Moh's Hardness Values (page 4)

Table 2: Common Mill Types (page 7)

Table 3: Moh's Hardness Values (page 29)

Table 4: List of d_{hkl} versus 2θ peaks for Al, Mg, Si, Zn, Zr (page 47)

Table 5: Moh's Hardness Values and Crystal Structures (page 66)

List of Abbreviations:

MA: Mechanical Alloying

BPR: Ball-to-Powder Ratio

PCA: Process Control Agent

MM: Mechanical Milling

XRD: X-ray Powder Diffraction

HEPA: High Efficiency Particulate Air

DS: Divergence Slit

SS: Scattering Slit

RS: Receiving Slit

FT: Fixed Time

CT: Count Time

CPS: Counts Per Second

Acknowledgments

First and foremost, I would like to thank my advisor, Professor Jason Trelewicz, for giving me the opportunity to work in his laboratory and for truly looking out for my best interests throughout this entire process.

Secondly, I would like to thank Olivia Donaldson, for teaching me how to use the planetary ball mill and the XRD, for helping me become a user at BNL, and for always being there to answer my questions. I genuinely appreciate your advice and guidance throughout these past two years.

I would also like to thank Professor Sanjay Sampath for not only being on my committee, but also for the experience I gained at the Center for Thermal Spray Research during my junior year. Without that research experience, I would have never gotten my first internship with GE Power.

Thank you, Dmytro Nykypanchuk at the Center for Functional Nanomaterials at Brookhaven National Laboratory for allowing me to use the Ultima III.

Thank you to the Department of Energy and to the National Science Foundation for funding this research.

A special thanks to Jim Quinn – who was the very first professor to see my engineering potential and to act on it. I certainly would not be where I am today without your guidance and support.

I would like to thank Christopher Thompson and Lawrence Levy from GE Power's Repair and Development Center in Greenville, SC for giving me the incredible opportunity to collaborate with them for my thesis work. Although it did not work out, I genuinely appreciate their willingness to help me with my thesis however they could.

And lastly, I would like to thank my family. Thank you for your support, love, and guidance throughout this process.

Chapter 1: Introduction

Nanocrystalline metals have useful mechanical properties such as high strength, improved wear resistance, and longer fatigue life [1-3]. The high strength property of nanocrystalline metals is due to the increase in the overall number of grain boundaries – this direct result of reducing a material's grain size hinders dislocation movement [4]. When grain sizes are around 15 – 100nm, dislocations being emitted from grain boundary sources is what dominates plasticity [5]. These dislocations travel across the grain until they are momentarily pinned at the ends of grain boundary sites where they are absorbed into the opposite grain boundary [5].

Naturally, the potential that nanocrystalline materials have in terms of producing these useful mechanical properties is limited by the high volume fraction of grain boundaries which also cause structural instability. Alloying has been used to limit grain growth by two different mechanisms: one being to treat grain boundary motion with second phase pinning or solute drag, the other being to remove the excess free energy stored within the grain boundaries by solute segregation [6-8]. When comparing these two mechanisms, the kinetic nature of the solute drag mechanism oftentimes causes nanocrystalline grains to coarsen, which may be sufficient for some applications, but not all [6]. Additionally, solute drag is heavily dependent upon temperature for mobility, so it is only effective at relatively low, homologous temperatures [6]. On the other hand, if the excess free energy within the grain boundary is removed via solute segregation to limit the driving force for grain growth, then nanocrystalline alloys can be developed reliably while maintaining their structures at higher temperatures, and this opens up a wider range of applications and processing routes [6]. Solute segregation, or solute doping, not

only reduces the grain boundary energy, but it has also been shown to enhance the strength of the nanocrystalline metal [9].

This thesis is partially based upon the work of Murdoch and Schuh, which uses a thermodynamic model to estimate grain boundary segregation enthalpy [10]. Their work suggests that magnesium has a positive enthalpy of segregation in aluminum and that if they were to be alloyed, magnesium would prefer to be at the grain boundaries [10]. $Al_{0.7}Mg_{0.3}$ was successfully synthesized via mechanical alloying in a planetary mill experimentally; the resulting X-ray Powder Diffraction peaks showed chemical mixing of magnesium into aluminum after milling for six hours [11]. This proves that: 1) mechanical alloying is a processing route for the solute segregation mechanism for stabilizing nanocrystalline metals, as mentioned previously; and 2) when a binary system does undergo chemical mixing according to the X-ray Powder Diffraction results, there is a chance that one element is stabilizing the ultrafine grain size of the other by residing within the ultrafine grained material's grain boundaries.

During mechanical alloying, extensive straining forces the chemical mixing between the powder constituents via co-deformation. Overall, this process is a function of the powder constituents' mechanical properties (most importantly, strength), microstructures, and chemical mixing [12]. By changing all three of these variables, two distinct behaviors of the powder system are noticed: they either become chemically homogenized, or they remain in dual phase – and this depends upon the base element's relative strength [12]. Currently, there is no "general quantitative heuristic" by which mixable, powder systems can be predicted (or definite conditions in which these powder systems can become mixable) [12]. However, it has been suggested that chemical mixing can be "encouraged" by either ensuring the co-deformation is between powders with relatively similar mechanical properties, and/or making sure the

microstructures of the powder constituents agree (in terms of volume fraction and geometry) [12]. For instance, when considering the impact of volume fraction, if there is a relatively hard element present, the softer element present can easily flow around the harder element without deforming the harder element [13]. However, that becomes more difficult if the volume fraction of the harder element increases. Therefore, the relative hardness of the constituent elements compared to the base-alloying element is important as to whether or not it chemically mixes and inevitably, if solute segregation within the grain boundaries occurs.

In order to determine whether or not a grain boundary can be doped with a certain element, it must be determined whether or not the solute and solvent can be chemically mixed. Within this thesis work, 99 atomic % aluminum 1 atomic % silicon, 99 atomic % aluminum 1 atomic % zinc, 99 atomic % aluminum 1 atomic % magnesium, and 99 atomic % aluminum 1 atomic % zirconium were ball milled with a Retsch Planetary Ball Mill under an argon atmosphere. As mentioned before, the work of Murdoch and Schuh suggests that magnesium has a positive enthalpy of segregation in aluminum and that if they were to be alloyed, magnesium would prefer to be at the grain boundaries, and this was proven experimentally by S.M. Umbraikar et al. [10,11]. So the chosen solvent was aluminum and the rest of the secondary/solute elements (silicon, zinc, and zirconium) were chosen based upon their Moh's hardness compared to that of aluminum, as seen in Table 1. X-ray Powder Diffraction was used to determine average crystallite size, strain within the powder particulates, and to determine whether or not each of the binary systems underwent chemical mixing.

Table 1: Moh's hardness values for each of the elemental powders used [14].

Element:	Moh's Hardness Value (MPa):
Aluminum	2.75
Magnesium	2.5
Silicon	6.5
Zinc	2.5
Zirconium	5

1.1. Materials Science Fundamentals

There are four fundamental concepts within materials science which apply to mechanical alloying and behind this thesis work: hardness, severe plastic deformation, cold welding and fracturing. Each of the secondary elements were chosen based upon their harnesses relative to aluminum (described in 1.1.1.), and within mechanical alloying, powder particles undergo severe plastic deformation (described in 1.1.2.), cold welding (1.1.3.), and fracturing (1.1.4.).

1.1.1. Hardness

Hardness is a measure of a material's ability to resist localized plastic deformation [15]. It is dependent upon the material's ductility, elastic stiffness, toughness, strain, strength, and viscoelasticity [15]. Hardness contains several different materials properties, and it is important because the degree to which the binary powders mix will be compared to each element's hardness value. As mentioned previously, chemical mixing can be "encouraged" by either ensuring the co-deformation is between powders with relatively similar mechanical properties, and/or making sure the microstructures of the powders agree. If the volume fraction of a

relatively soft metal compared to that of a relatively hard metal is low, then the likelihood of chemical mixing is higher. If, either, the relative hard metal's hardness is too high and/or the volume fraction is higher, the likelihood of mixing is therefore lower. Therefore, the relative hardness of the constituent elements compared to the base-alloying element (or the solvent element) is important as to whether or not it chemically mixes and inevitably, if solute segregation within the grain boundaries occurs.

1.1.2. Severe Plastic Deformation

Severe plastic deformation describes goes on during a metallic processing technique that involves very large strains undergoing very large shear stresses which results in a very high density of defects and ultrafine grained materials. This is the type of deformation which occurs during mechanical alloying; it creates the large amount of defects within the metallic powders: the vacancy concentration drastically increases, the amount of dislocations drastically increases, and new high angle grain boundaries are formed [16]. The creation of these new defects, along with internal stress from this plastic deformation, can promote phase transformations such as solid state amorphization, disordering, or dissolution of precipitates [16].

1.1.3. Cold Welding

Occurs during the first stages of mechanical alloying, cold welding is a solid-state welding process which joining of particles takes place without heat or a fusion interface [1]. It does not require the powder particles to be in a liquid state or in a molten phase – it does, however, require very large pressures[1]. It is what causes an increase in the diameter of the powder particles, which is reduced during fracturing.

1.1.4. Fracturing

Fracturing occurs when a material is separated into two or more parts undergoing stress and/or pressure. It is what reduces the effect of cold welding that occurs during mechanical alloying; it occurs due to crack propagation that slowly moves across the material and is usually followed by a large amount of plastic deformation [1,15].

1.2. Synthesis – Mechanical Alloying (MA)

The aluminum-silicon, aluminum-zirconium, aluminum-magnesium, and aluminum-zinc powders were synthesized via mechanical alloying in a planetary ball mill. Mechanical alloying (MA) is a solid-state powder metallurgy processing technique which essentially involves the cold welding, fracturing, and rewelding of powder [17]. MA enables the alloying of several different powders to create unique phases. One of the greatest advantages of MA is that it can alloy elements which are normally immiscible, which is not possible with any other processing technique [18]. This process was developed by John Benjamin and his colleagues at the Paul D. Merica Research Laboratory within the International Nickel Company in order to produce nickel-based superalloys for gas turbine applications in 1966 [17]. Mechanical alloying is a relatively inexpensive and simple technique which is ideal for powder processing because it enables the user to process powders under non-equilibrium conditions. By "energizing and quenching" materials during processing under non-equilibrium conditions like mechanical alloying, the unique and desired materials properties can be obtained by rapidly cooling said material.

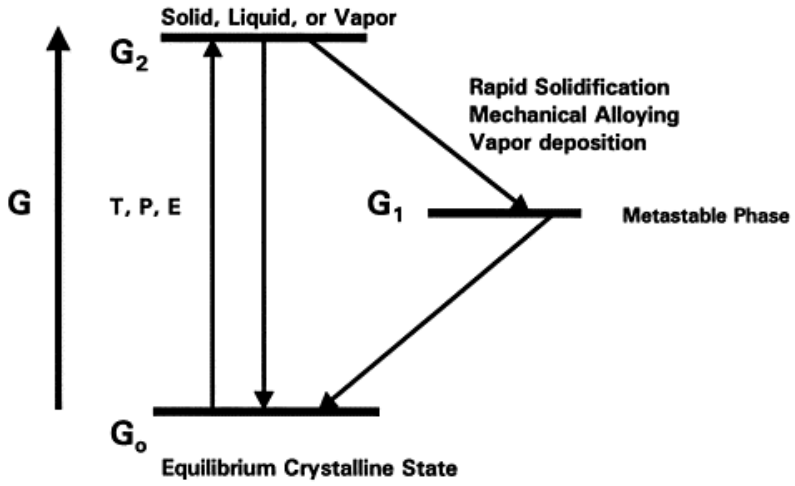

Figure 1: Non-equilibrium synthesis by "energizing and quenching" used in multiple materials processing techniques (rapid solidification, mechanical alloying, vapor deposition) [17].

1.2.1. Mechanical Alloying Variables

Mechanical alloying is a complex process which involves optimizing several variables to achieve the desired microstructure and/or phase. Some important parameters that effect the final powder's properties include:

- Type of mill (1.2.1.1.)
- Milling speed (1.2.1.2.)
- Milling container (1.2.1.3.)
- Milling time (1.2.1.4.)
- Type and size of grinding medium (1.2.1.5.)
- Percent of empty space in the jar (1.2.1.6.)
- Milling atmosphere (1.2.1.7.)
- Ball-to-powder ratio (1.2.1.8.)
- Process controlling agent (1.2.1.9.)
- Temperature of milling (1.2.1.10.)

All of these variables are not necessarily independent of each other (i.e. the ideal milling time depends upon the size of the grinding medium, the type of mill, the ball-to-powder ratio, etc.) and will be discussed in more detail in the following sections.

1.2.1.1. Type of Mill

There are several different mills that one can use for MA. They differ in milling speed, jar capacity, and ability to vary the milling temperature in order to minimize powder contamination [17]. Table 1 lists some common mill types and an allowable sample weight. The powder type, powder quantity, and the final constitution of the powder dictates which mill is ideal for the powder processing. For instance, planetary ball mills or attritors are used to produce large quantities of powder, while shaker mills are used for alloy screening purposes [17]. In certain specific applications, specially designed mills are used (and are not included in Table 2).

Table 2: Common mill types and their allowable capacities (sample weights) [17]

Mill Type:	Sample Weight:
Mixer Mills	Up to 2 x 20 g
Planetary Mills	Up to 4 x 250 g
Attritors	0.5 – 100 kg
Uni-Ball Mill	Up to 4 x 2000 g

1.2.1.2. Milling Speed

The faster the mill rotates, the higher the energy input into the powder would be. The maximum speed of the mill is restricted upon what type of mill is used, and above a certain critical speed, the grinding media will be pinned to the inner walls of the milling jar, they do not fall down, and as a result, they do not exert any impact force upon the powder [17]. In order to deliver the highest energy input to the powder, the maximum speed should hit the critical value

such that the grinding media falls from a maximum height to produce the desired maximum collision energy [17]. The temperature increase that naturally comes with faster speeds may be a disadvantage, and will therefore limit the maximum speed for those reasons. Higher temperatures from faster speeds are ideal in cases where diffusion is required to promote alloying [17]. The increase in temperature can be a disadvantage in cases that decomposition of the supersaturated solid solutions/metastable phases that have been formed occurs [17]. Additionally, higher speeds also increase the likelihood of contamination because of the jar's temperature increase [17].

1.2.1.3. Milling Container

Milling jars are typically made of hardened steel, hardened chromium steel, tool steel, tempered steel, tungsten carbide, tungsten carbide cobalt, stainless steel, and bearing steel [17,18]. The material that is used to make the milling jar is important because the some of the milling jar material will contaminate/be incorporated into the chemistry of the final powder. The shape of the jar may also affect the rate at which alloying occurs. In a study by J.L. Harringa, B.A. Cook, and B.J. Beaudry, alloying occurred within their flat-ended SPEX mill container significantly higher than the round-ended SPEX mill container (the time to achieve the (111) peak of Si-Ge was 9 hours for the flat-ended container and 15 hours for the round-ended container) [19].

1.2.1.4. Milling Time

The duration of milling is chosen as to achieve a steady state between fracturing and cold welding of the powder particulates. Milling time is an important parameter. The ideal time is dependent upon several factors: type of mill used, ball-to-powder ratio, the milling temperature,

and the milling intensity/speed [17]. Because the level of contamination increases with milling time (along with some potentially undesirable phases), the milling time should last for the required duration, and not any longer than that.

1.2.1.5. Type and Size of Grinding Medium

The most common materials used for the grinding medium are stainless steel, hardened steel, hardened chromium steel, tool steel, tempered steel, bearing steel, and tungsten-carbide cobalt [17]. In order to create enough of an impact force on the powder, the density of the grinding medium should be high. The grinding medium and the milling jar should be made of the same material whenever possible in order to reduce the amount of cross contamination.

The milling efficiency is influenced by the diameter/size of the grinding medium. High density grinding medium with larger sizes will generally transfer more impact energy to powder particles [17]. However, according to multiple studies, larger sized grinding media is not ideal when trying to achieve an amorphous phase. In a set of investigations, an amorphous phase of titanium-aluminum alloys was produced faster while using 3/16" diameter steel balls than using 3/4" diameter balls [20,21]. In fact, only a stable crystalline compound of titanium-aluminum was produced when milling was done with larger diameter steel balls [20]. In another study, an amorphous phase of titanium-aluminum was only formed when 5mm or 8mm balls were used for milling; when using 12mm balls, an amorphous phase did not form [21,22]. A very similar result occurred when milling palladium-silicon – an amorphous phase of that powder system was favored when smaller media was used [23]. It was suggested that the reasoning behind this is because smaller sized media produced more intense frictional action which in turn promoted

amorphization [22]. "Soft" milling conditions (smaller media size, lower energies, and lower ball-to-powder ratios) seem to enable metastable phase formation/amorphization [22].

Throughout mechanical alloying investigations and research, it is common to see only one size of grinding medium used. There have been a few instances where the researchers decided to use different sized media. It was predicted by Gavrilov et al. that the highest collision energy can be achieved if different sized media was used [24]. In the beginning stages of milling, the surface of the grinding medium gets coated with powder; and in some circumstances, the powder cold welds to the grinding medium [17]. The overall thickness of this coating layer should always try to be minimized in order to prevent a ball-powder heterogeneous product from forming [24]. Unfortunately, it is difficult to detach the powder from the media, so it can lead to low powder yields [17,24]. By combining both large and small media sizes, it has been reported that it minimizes the coating of powder formed on the media's surface and it minimizes the potential for powder cold welding to the media's surfaces [25,26]. This can possibly be because the shearing forces that are produced by different sized media may help detach powder from the media's surface [17].

Additionally, to ensure that the motion of the grinding media is randomized, combining smaller and larger media sizes is necessary [27]. Using the same sized grinding media (regardless of jar type) has been shown to produce tracks [17]. It is more ideal to have the media hit surfaces randomly than it is to have them traveling along a well-defined trajectory.

1.2.1.6. Percent of Empty Space in Jar

There has to be enough empty space in the jar in order for the impact forces of the grinding media to be exerted on the powder; it is necessary for there to be enough empty space

for the media and the powder particles to move around [17]. If there is too much free space, then the quantity of powder is not maximized. If there is too little room in the jar, then there is not enough free space for the media to move around, so the impact energy of the media is less. The percentage of empty space necessary in the jar depends upon the manufacturer's recommendations. Generally, about 50% of the jar space is left empty [17].

1.2.1.7. Milling Atmosphere

If the milling atmosphere is not controlled, contamination of the powder can also occur (mostly due to oxygen present – it can cause oxidation and/or oxides). Powders are typically milled in containers that either have been evacuated or in inert gas atmospheres (such as argon or helium) [17]. High purity argon is the most commonly used to prevent oxidation and/or contamination of the powder.

1.2.1.8. Ball-to-Powder Ratio (BPR)

The ball-to-powder ratio (BPR) has a significant effect on the milling time required in order to achieve a certain phase in the powder. Researchers have experimented with ratios as low as 1:1 and as high as 220:1 [17]. The higher the BPR, the shorter the time to achieve the desired results. For example, in a study done by C. Suryanarayana, G.H. Chen, and F.H. Froes, an amorphous phase of Ti-33 atomic % Al powder mixture was milled in a SPEX mill with a BPR of 10:1 in 7 hours, and that same powder mixture became amorphous within just 1hr with a BPR of 100:1 [28]. The number of collisions per unit time increases with an increasing BPR because more energy is transferred from the grinding media to the powder (alloying occurs much, much faster). The temperature of the jar increases with higher BPR due to more frictional forces, this can also change the resulting powder (had there been more heat in the jar, the

amorphous powder in C. Suryanarayana's study could have crystallized) [17,20]. Higher BPR, a "hard" condition, produces equilibrium phases, while lower BPR, a "soft" condition, produces metastable phases [17].

1.2.1.9. Process Controlling Agent (PCA)

Alloying during milling can be disrupted if powder particles cold weld to one another. The heavy plastic deformation which the powder particles experience (especially in cases where the powder particles are ductile) is what causes the cold welding. A balance of fracturing and cold welding must be maintained. A process control agent (PCA) (which can also be referred to as a a surfactant or a lubricant) is commonly added to the powder before mixing in order to reduce the effect of cold welding. PCAs can be solids, liquids, or gases – they are usually (but not necessarily) organic compounds that are absorbed onto the surface of the powder particles [17]. This lowers the surface tension of the solid material, which thereby reduces the likelihood of cold welding which in turn, reduces unwanted powder agglomeration. *E*, the energy that is physically required for the size reduction process, is given by:

$$\boldsymbol{E = \gamma \cdot \Delta S}$$

where γ is the specific surface energy and ΔS is the change (or increase) in surface area. By reducing surface energy, it results in shorter milling times and/or the generation of powders with smaller diameters.

Typically, 1-5 wt% of PCAs are added to the powder mixture [17]. There are several different kinds of PCAs that one can use, the most important ones that are used, however, include: ethanol, methanol, hexane, and stearic acid [17]. Some other exotic PCAs can be used, including: trichlorotrifluoroethane, didocyldimethyl ammonium bromide (DDAB), diodecyl

dimethyl ammonium acetate (DDAA), lithium-1,2-bis-dodecyloxy carbonyl sulfasuccinate, sodium-1,2-bis(dodecyl carbonyl)ethane-1-sulfonate, polyethylene glycol, ethyl acetate, boric acid, oxalic acid, alumina, and aluminum nitrate [17]. Most of the PCAs used decompose during milling, they sometimes they interact with the powder and form compounds, and these become inclusions and/or dispersoids into the powder particles during the milling process [17]. The carbohydrates and hydrocarbons found within the PCAs are likely to introduce oxygen and/or carbon into the powder particles. This results in the formation of oxides and carbides that are evenly distributed within the matrix [17]. Luckily, this is not typically harmful to the alloy system because the addition of the carbides and oxides contribute to the dispersion strengthening of the material, which means the powder particles have increased strength and increased hardness [29]. Hydrogen from the PCAs typically escapes as a gas, or it can be absorbed into the metal lattice on sintering or heating [17]. Most of the time, hydrogen does not usually participate in the alloying process, it primarily acts as a surfactant [30].

The type of PCA and the quantity used determines the powder's final shape, size, and purity. A larger quantity of PCA typically reduces the powder particle's size by two to three orders of magnitude. In a study done by Lu and Lai, the milling of aluminum for 5 hours with 1 wt% stearic acid added produced a particle size of around 500 microns [31]. When 3 wt% of stearic acid was added to a 5 hour run, the aluminum powder size was only around 10 microns [31]. This makes sense because the more of the process control agent there is, the less likely that cold welding (a solid-state process which increases the powder particle diameter) will occur.

The purity of the final powder product and the nature of the desired powder being milled is what determines which PCA one should use. The amount of PCA and the type of PCA will determine the final powder yield and particle size. The overall effectiveness of the PCA can

actually be determined by the total powder yield after mechanical alloying. If the powder yield is high and the jar is cleaned out properly, it can be concluded that the PCA was effective. If the powder yield is low and the weight of the cleaned media after mechanical alloying is significantly more than before mechanical alloying, it can be concluded that the PCA is not effective. For instance, in the same study by Lu and Lai, it was found that 100% of the powder was recovered after milling for 15 hours when using 2 wt% stearic acid, but only 50% of the powder was recovered if 2 wt% polyethylene glycol was used [31].

All milling conditions and circumstances are different; there is no "universal" PCA that one can use. The amount of PCA that should be used is dependent upon the amount of powder and the grinding medium used, the thermal and chemical stability of the PCA, and the cold welding characteristics of the powder [17]. One must also decide on the PCA by looking at all possible interactions between the PCA and the metal.

1.2.1.10. Temperature of Milling

The milling temperature is another important parameter because temperature regulates diffusion processes, which thereby dictates the final constitution of the milled powder. Diffusion is heavily involved in the formation of alloys – so the milling temperature has a significant effect.

The milling temperature was intentionally varied in only a few studies. The temperature can be lowered by dripping some liquid nitrogen into the milling jar and the temperature can be increased by heating the jar electrically [17]. In a study by Hong et al., the root mean square strain was lower and the grain size was found to be larger during the formation of nanocrystals at higher milling temperatures [32]. Solid solubility has been shown to decrease at higher milling

temperatures. While planetary ball milling Cu-37at%Ag powder mixture, a crystalline supersaturated solid solution and an amorphous phase were obtained while milling at room temperature; however, only a Cu-8at%Ag solid solution was achieved when milling the powder at 200°C [33]. Increased diffusivity and the effects of equilibrium at higher milling temperatures was given for the decrease in solid solubility.

In mechanical alloying, higher milling temperatures enhance the kinetics of amorphization because higher temperatures enable diffusion processes to take place – as explained in 1.3. Mechanism of High Energy Milling, in order to achieve an amorphous phase in MA, a micro-diffusion couples must be formed of the constituent powders, and this should be followed by a solid state amorphization reaction. Higher temperatures have led to the amorphization of nickel-titanium and nickel-zirconium systems because they went through a mechanical alloying process [34,35]. It should be mentioned that during mechanical milling (MM) processes, it has been shown to be more ideal for the temperature to be lower in order to achieve an amorphous phase [17]. The difference between MA and MM is that MA enables the alloying of powder mixtures and material transfer is required to reach homogenizaton, while MM involves the milling of powders with a uniform composition (i.e. pure metals, intermetallics, etc.) and material transfer is not required for homogenization [17]. In MM, the powders are already alloyed, so the milling time required compared to MA is about half [17]. The reason why MM favors lower temperatures for amorphization is because it occurs by a different mechanism as compared to MA. During MM, amorphization occurs due to the increase in free energy in the crystalline phase which is caused by the introduction of defects (increased grain boundary area or anti-site chemical disorder) that occur while forming a nanocrystalline structure [17]. Thus, it is expected that lower milling temperatures are expected to favor the formation of an amorphous

phase. However, depending upon the powder being milled, both increased and decreased temperatures have been reported to favor amorphization by MM, even with the same powder composition [17]. For instance, when miling nickel titanium, it was reported that a shorter milling time was required for amorphization at 170°C than it was at 60°C [34]. Interestingly, Koch et al. reported reduced amorphization kinetics with increased milling temperature [35,36]. They reported it that it took 18 hours of milling to reach an amorphous phase at a milling temperature of 220°C, while it only took 2 hours to reach an amorphous phase at liquid nitrogen temperature [35,36]. The results Koch et al. reported were understood to be that amorphization took place due to increased grain boundary energy through the formation of a nanocrystalline structure, and that this nanocrystalline structure formed at lower milling temperatures [35,36]. The increase in milling time required for several intermetallics (including nickel titanium) with an increase in milling temperature can be seen in Figure 2.

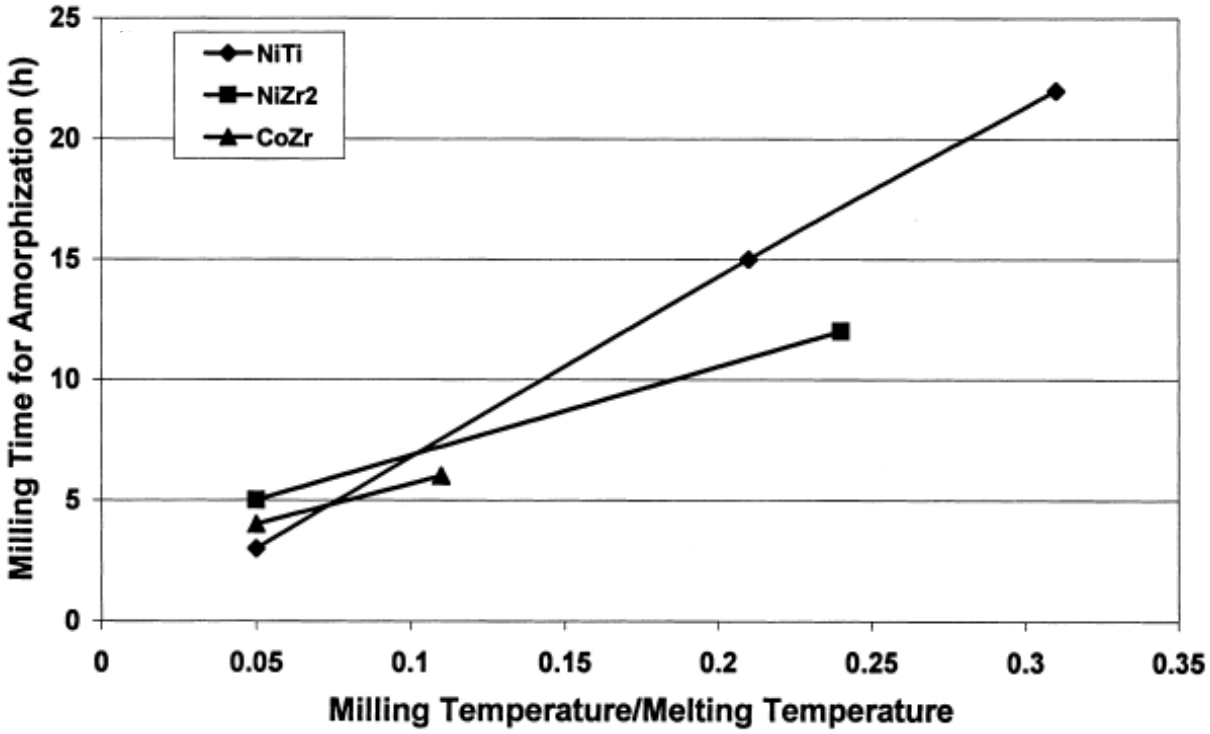

Figure 2: Plot of milling time required for amorphization versus the normalized milling temperature ($T_{milling}$ / $T_{melting}$) for NiTi, $NiZr_2$, and CoZr [17]. The increase in normalized temperature is directly related to milling time required for all three intermetallics.

1.3. Mechanism of Alloying – High Energy Milling

Powder particles are repeatedly flattened, cold welded, fractured, and then rewelded during high energy milling. Whenever there is a collision between two malls, some powder will be trapped in between them, as demonstrated in Figure 3 [17].

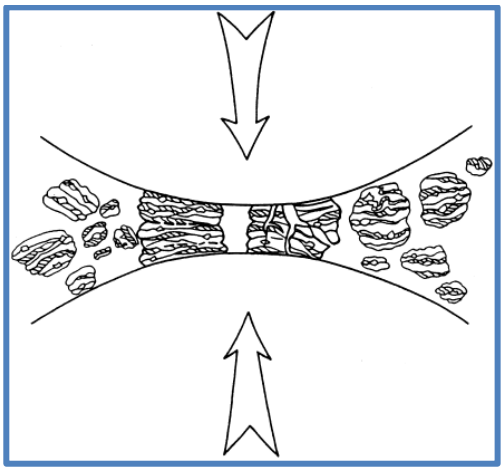

Figure 3: A schematic of the collision between the ball and powders during MA [17]. This collision is what leads to some powder being trapped on the ball's surface and the severe plastic deformation of the powder particles.

Approximately 1000 particles with an approximate weight of 0.2 mg are trapped during every collision – it is the force of this impact which causes the plastic deformation of powder particles, leading to fracture and work hardening [17]. Cold welding occurs because the new surfaces that are created allow for welding between the particles to occur – and this is what leads to an increase in particle size [17]. During the beginning of the milling run, the powder particles are pretty soft (during the milling of ductile-ductile powders and ductile-brittle powders). Because of this, the likelihood of the powder to weld together and form larger particles is high and a broad range of powder particle diameters develops – some diameters are even three times larger than the starting powder (from points **a** to **b** in Figure 4) [17]. The structure of these new, larger powder diameters have a layered structure that consists of various combinations of the original powder constituents (which can also be seen in Figure 3). As the deformation continues, particles experience work hardening and fracture by the fragmentation of fragile flakes and/or a fatigue failure mechanism [17]. It is at this stage that the likelihood of fracture is more than the likelihood of cold welding and the average particle size drops (from points **b** to **c** in Figure 4).

Eventually, the structure of the particles is steadily refined, due to the continued impact of the grinding medium, but then the particle size stays around the same [17]. As the plastic deformation continues, the spacing between the powder particle's layers decrease and the number of layers the particle has increases [17].

In a conventional ball mill, the efficiency of the particle size reduction that occurs is >0.1% [17]. Despite the fact that the efficiency is higher in high energy ball milling processes, the efficiency there is still less than 1% [17]. Most of the energy is lost as radiating heat; a small amount is utilized in the elastic deformation and the plastic deformation of the powder particles.

A steady-state equilibrium is reached after milling for a certain period of time when the rate of welding (that causes the increase of the average particle size) and the rate of fracturing (that decreases the average particle size) is about equal (from points **c** to **d** in Figure 4). Smaller particles tend to be able to survive the impact of the grinding media without fracturing; however, eventually, they tend to weld into larger pieces which eventually drive both the very large and the very small/fine particles towards an intermediate size [37]. It is when this occurs that every particle contains all of the starting ingredients, with the proportions that they were mixed together [17]. Due to the accumulation in strain energy, the particles reach a saturation hardness and at this stage, the size distribution of the powder particles is small – the particles which are larger than the average experience a reduction in size at the same rate that the smaller particles grow through agglomeration with other smaller particles [17]. A graph of the particle size with respect to milling time can be seen in Figure 4:

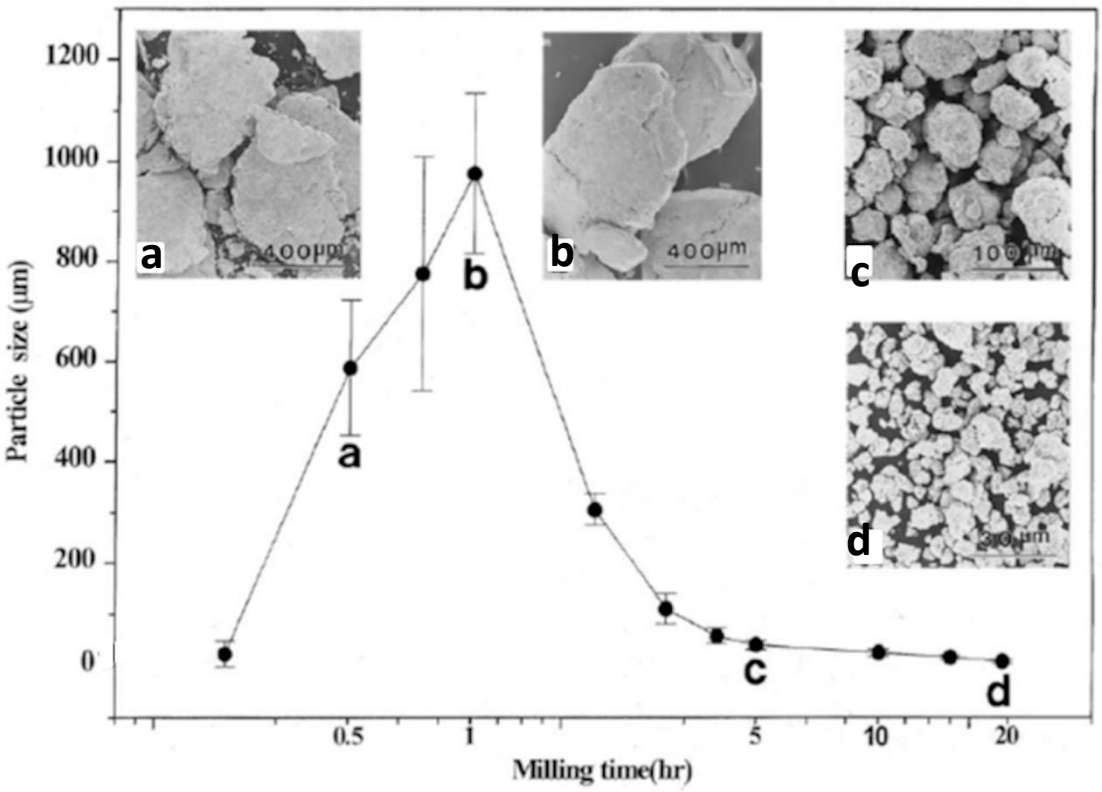

Figure 4: General relationship between the average particle size and the milling time [17]. **Points a to b:** In the beginning of a milling run, the powders tend to weld together and create larger particles (the rate of particles welding is much greater than the rate at which particles are fracturing), so the average particle size increases. **Points b to c:** As the powder particles experience more deformation, the powders experience work hardening and fracturing, so the rate at which the powders fracture is much less than the rate at which they are welding; therefore, the average particle size is decreasing. **Points c to d:** Represents the equilibrium that the milling process eventually experiences – the rate of welding is equal to the rate of fracturing because the particles which are larger than the average experience a reduction in size at the same rate that the smaller particles grow through agglomeration with other smaller particles.

Clearly, the powder particles experience severe plastic deformation during the process of MA. This severe plastic deformation results in the presence of a variety of crystallographic defects within the powder particles, including: dislocations, stacking faults, vacancies, and an increased number of grain boundaries [17]. The presence of these defects is actually beneficial because not only does it it enhances the diffusivity of the solute elements into the solvent's

matrix, but it also decreases the distance needed for diffusion due to refined microstructural features [17]. This rise in temperature leads to the true alloying of the powder constituents.

While the alloying that takes place during MA generally occurs at room temperature, sometimes it is necessary for the powders to undergo annealing at an elevated temperature in order for the alloying to be achieved. The elevated temperatures during annealing further aid the powder's diffusion behavior, which will enable the desired alloying to occur. This is usually necessary for some intermetallics that undergo MA [17].

The time required to form any given structure in any system is a function of the powder particle's initial size, the characteristics of the powder's ingredients, the equipment that is being used for MA, and the equipment being used to control the operating parameters. In most cases, the rate at which the internal structure (i.e. particle size, lamellar spacing, crystallite size, and etc.) is being refined has a roughly logarithmic scale with the chosen processing time [17]. Because of this relationship, one can conclude that the size of the starting powder particles is basically irrelevant. During the beginning of the MA run, the grain size is reduced to nanometers and the lamellar spacing usually becomes small, as seen in Figure 5 [17]. Nanostructured materials are easily synthesized with MA, which is why MA is extensively used to create nanocrystalline materials [17].

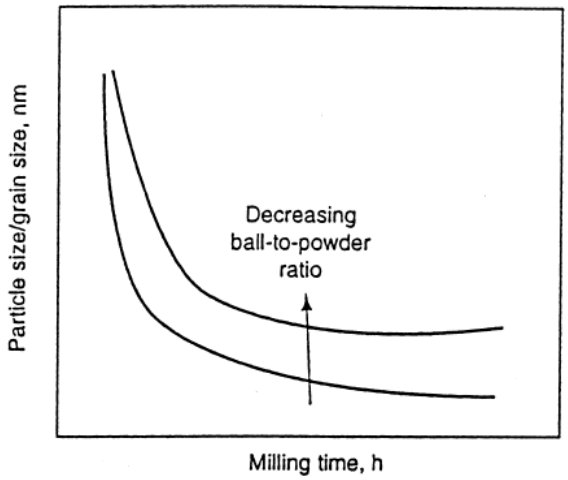

Figure 5: A schematic representing the logarithmic relationship between milling time in hours versus particle size (or grain size) in nanometers [17]. As mentioned before, the rate of refinement of the powder particles increases with a decreasing ball-to-powder ratio, higher energy milling, lower temperature, and etc.

It is possible to conduct MA in three different combinations of metals and alloys: ductile-ductile, ductile-brittle, and brittle-brittle. Because aluminum-silicon, aluminum-zirconium, aluminum-magnesium, and aluminum-zinc are either ductile-ductile or ductile-brittle, the mechanism of MA during those two combinations will be discussed in the following two sections.

1.3.1. Ductile-Ductile MA Systems

Ductile-ductile MA systems are the most ideal combination of materials for MA. It has been suggested that it was necessary to have at minimum 15% of a ductile component in the milling jar in order to achieve alloying [37]. This is because, as mentioned earlier, true alloying occurs due to the welding and fracturing of particles repeatedly, and cold welding cannot occur if the powders lack ductility [17].

The mechanism of alloying in a two different ductile component system was described by Benjamin and Volin [38]. They suggested that in the earlier stages of MA, the ductile components get flattened into a pancake/platelet shape via a micro-forging process. A small amount of powder (with a thickness of one to two particles) gets welded onto the media's surfaces. The forming of this coating is ideal because it prevents excessive wear of the grinding medium and it prevents the contamination of powder by the grinding medium. However, although it is advantageous, this coating on the grinding medium should be kept to a medium in order to reduce the likelihood that the grinding medium and the powder form a heterogeneous final product [24]. In the next stage of MA, the pancake/platelet like particles cold weld to one another to form a composite with a lamellar structure of the original constituents. During this stage, the the particle size is expected to increase. As the MA time is increased, the composite powder particles undergo work hardening, and consequently, the hardness and the brittleness of the powders increase, so the powder size decreases, resulting in powders with more equiaxed dimensions. Afterwards, the elemental lamellae eventually becomes more convoluted rather than linear, as seen in Figure 6.

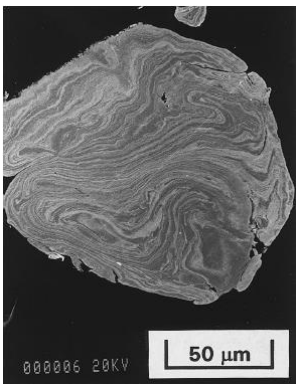

Figure 6: Scanning electron micrograph of the convoluted lamellar layer of a ductile-ductile component system (Ag-Cu) [17].

This happens because equiaxed powder is randomly welded together without any particular preference to the orientation in which welding occurs. At this stage, welding begins to occur because of the combination of increased lattice defect density, decreased diffusion distances (interlamellar spacing), and any heating that may have happened during milling. The particle size and hardness tend to reach saturation at this point – it is often referred to as the steady-state processing stage. True alloying occurs at the atomic level with further milling, and this results in the formation of intermetallics, solid solutions, and/or amorphous phases. The spacing between lamellar spacing becomes so fine (or it appears to disappear) that this stage; it becomes no longer visible under an optical microscope. One can tell that the MA process has been completed (a homogenous structure in the powder has been attained), when the powder can be removed from the grinding medium [1].

1.3.2. Ductile-Brittle MA Systems

Another MA system found within this thesis work is ductile-brittle. The microstructural evolution of the MA of ductile-brittle system has been described by Benjamin and others [24,39]. The ductile component flattens during the initial powder-ball collisions, while the brittle particles get fragmented/comminuted as seen in Figure 7.

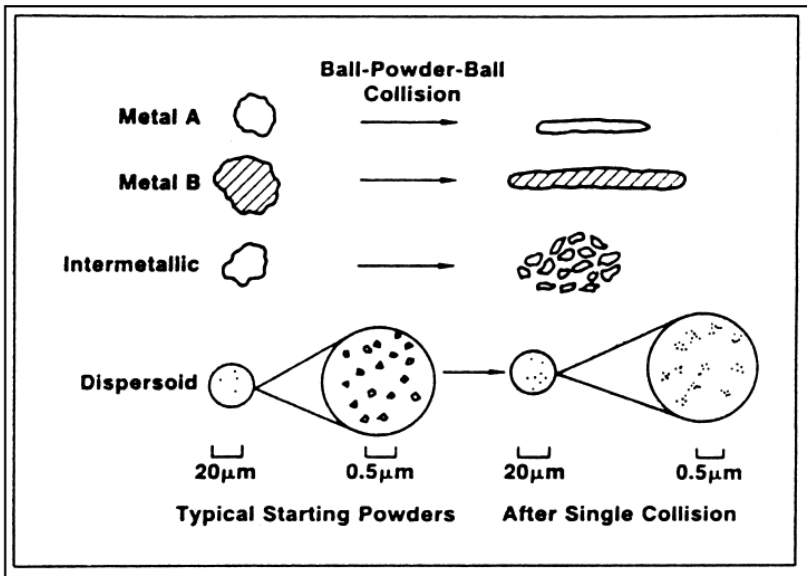

Figure 7: Typical deformation characteristics of some representative constituents of starting powders that is used in MA [17].

During the earlier phases of MA, the brittle, fragmented particulates tend to become trapped in the ductile particles and become occluded by the ductile particles. The brittle constituents tend to be trapped and closely spaced along the interlamellar spacings, as seen in Figure 8(a). As the milling time increases, the ductile powders experience work hardening, the lamellae get convoluted and refined (which is to be expected) – each individual particle's composition begin to converge toward the overall composition of the starting powder's blend as seen in Figure 8(b). Eventually, the lamellae gets further refined as the milling time continues to increase, the spacing between interlamellar spaces decreases, and the brittle particulates get evenly dispersed throughout if they are insoluble within the ductile powder's matrix (as seen in Figure 8(c)). Figure 9 is a transmission electron microscopy image showing a generally uniform dispersion of Er_2O_3 particles within MM α_2-titanium aluminide alloy matrix (the case where the brittle component is not soluble with the ductile matrix).

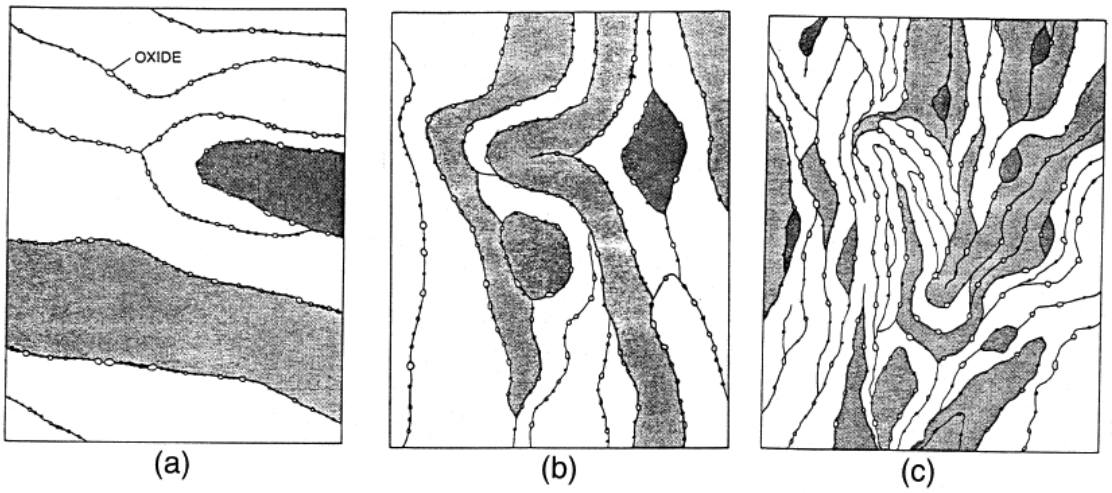

Figure 8: The structural evolution during MA of ductile-brittle systems of powders [1]. (a) Brittle particles tend to become trapped within ductile particles in early stages of MA; (b) Ductile powder experiences work hardening and lamellae gets further refined, the brittle particles become further refined; (c) If the brittle powder is insoluble with the ductile powder's matrix, the lamellae will get further refined, the interlamellar spacing decreases, and the brittle particles are evenly dispersed throughout [17].

If the brittle phase is in fact soluble within the ductile powder's matrix, alloying will occur between both components and the desired chemical homogeneity is achieved. An example of a ductile-brittle powder system in which the brittle component is soluble with the ductile matrix is $NiZr_2$ (brittle) in pure Zr (ductile) [40]. Alloying of ductile-brittle powder systems during MA requires simply the fragmentation of brittle particles in order to initiate short-range diffusion, but additionally, a reasonable solid solubility within the ductile component's matrix.

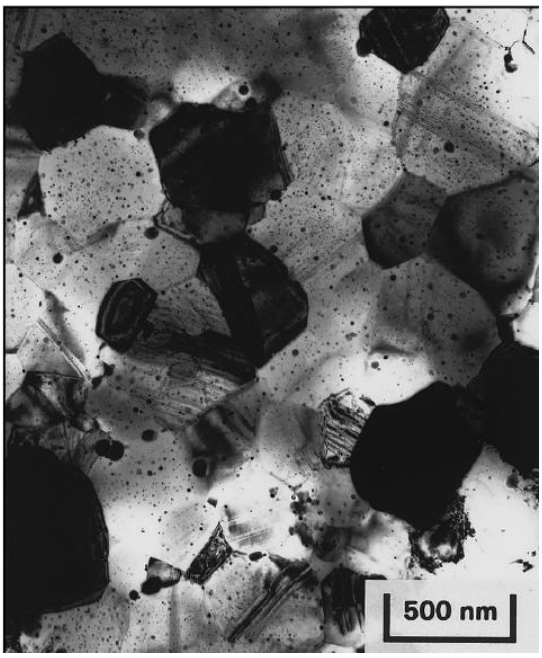

Figure 9: Transmission electron microscopy image showing a generally uniform dispersion of Er_2O_3 particles within MM α_2-titanium aluminide alloy matrix (the case where the brittle component is not soluble with the ductile matrix).

1.3.3. Planetary Ball Mill

In order to produce MA powders, different types of high-energy milling equipment can be used. Because this research involves the use of a planetary ball mill, the specifics about this type of mill will be explained in this section. A planetary ball mill, also referred to as Pulverisette, is a popular mill for conducting MA. It can only mill a few hundred grams of powder at a time [1]. They are currently being manufactured by Retsch in Germany (pictured in Figure 10) and Fritsch GmbH in Germany, which is marketed by Gilson Co., in the United States and Canada [17,41]. The name of this mill was given for the planet-like movement of its vial(s) [17]. The vials are rotated on a support disk (which it revolves like the Earth would around the Sun) and a special drive mechanism also causes them to rotate around their own axes, as seen in Figure 11 [17].

Figure 10: Retsch PM100 Planetary Ball Mill used within a glove box to mill the Al-Si, Al-Zn, Al-Mg, and Al-Zr powder systems [42]. This ball mill only has only 1 grinding station.

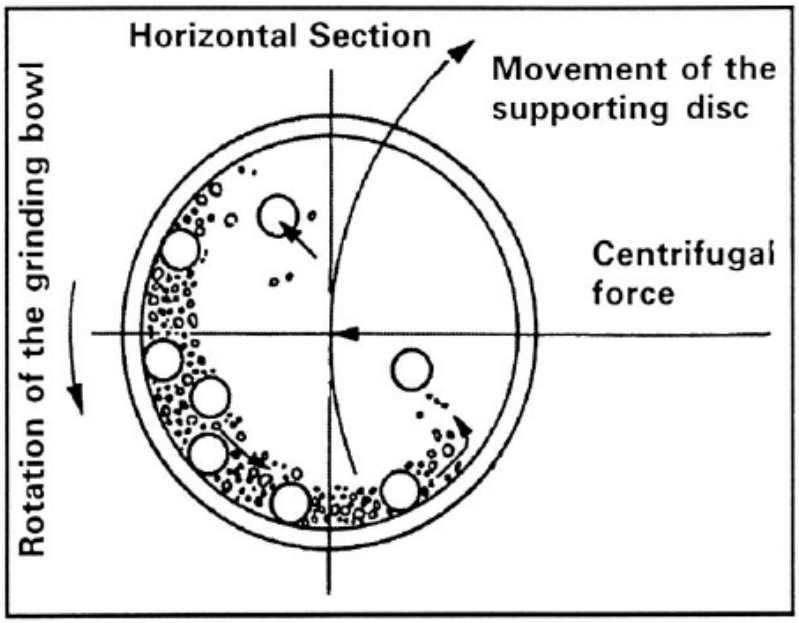

Figure 11: Schematic of a planetary ball mill in motion [17]. Shows the planetary-like motion of the balls where the jar rotates along its own axis and the entire jar revolves in the direction of the movement of the supporting disk.

When comparing to a SPEX mill, the linear velocity of the media in a planetary ball mill is faster than that of a SPEX mill; however, because the frequency of impacts that occur within a SPEX mill is greater than that of a planetary ball mill, a planetary ball mill can be considered a lower energy mill [17]. Additionally, the estimated temperature rise within the SPEX mill is less than that of a planetary ball mill. With a Ni-Zr system, it was estimated that a SPEX 8000 mill would cause a temperature rise 180°C [43]. With a Ni-Al system, it was estimated that a planetary ball would cause a temperature rise of 220°C [44].

1.4. Problem Statement

Nanocrystalline metals have useful mechanical properties such as high strength, improved wear resistance, and longer fatigue life [1-3]. Despite their potential, nanocrystalline metals are relatively unstable and can be easily subjected to rapid grain growth. After comparing

the work of Murdoch and Schuh, which used a thermodynamic model to estimate grain boundary segregation enthalpy to the experimental work of Umbrajkar et al., it was realized that nanocrystalline powders can be stabilized via grain boundary doping though mechanical alloying [10,11]. In order to determine whether or not a grain boundary can be doped with a certain element, it must be determined whether or not the solute and the solvent will chemically mix. Within this thesis work, 99 atomic % aluminum 1 atomic % silicon, 99 atomic % aluminum 1 atomic % zinc, 99 atomic % aluminum 1 atomic % magnesium, and 99 atomic % aluminum 1 atomic % zirconium were ball milled with a Retsch Planetary Ball Mill under an argon atmosphere. As mentioned before, the work of Murdoch and Schuh suggests that magnesium has a positive enthalpy of segregation in aluminum and that if they were to be alloyed, magnesium would prefer to be at the grain boundaries, and this was proven experimentally by S.M. Umbraikar et al. [10,11]. The rest of the secondary elements (silicon, zinc, and zirconium) were chosen based upon their Moh's hardness compared to that of aluminum, as seen in Table 3. X-ray Powder Diffraction was used to determine average crystallite size, strain within the powder particulates, and to determine whether or not each of the binary systems underwent chemical mixing.

Table 3: Moh's hardness values for each of the elemental powders used [14].

Element:	Moh's Hardness Value (MPa):
Aluminum	2.75
Magnesium	2.5
Silicon	6.5
Zinc	2.5
Zirconium	5

Chapter 2: Materials and Methods

The following section discusses the powders used in this thesis and provides general procedures for both ball milling and X-ray powder diffraction. Additionally, necessary calculations and chosen parameters are provided and described for both ball milling and X-ray powder diffraction.

2.1. Materials – Binary Systems

In order to determine whether or not a grain boundary can be doped with a certain element, it must be determined whether or not the solute and solvent will chemically mix. As mentioned before, the work of Murdoch and Schuh suggests that magnesium has a positive enthalpy of segregation in aluminum and that if they were to be alloyed, magnesium would prefer to be at the grain boundaries, and this was proven experimentally by S.M. Umbraikar et al. [10,11]. Within this thesis work, 99 atomic % aluminum 1 atomic % silicon, 99 atomic % aluminum 1 atomic % zinc, 99 atomic % aluminum 1 atomic % magnesium, and 99 atomic % aluminum 1 atomic % zirconium were ball milled with a Retsch Planetary Ball Mill under an argon atmosphere. The powders were acquired from the following: aluminum powder from Alfa Aesar with a 99.5% purity and a mesh size of -325, magnesium powder from Alfa Aesar with a 99.8% purity and a mesh size of -325, silicon powder from Alfa Aesar with a 99.5% purity and a mesh size of 325, zinc powder from Alfa Aesar with a 99.9% purity and a -140 to 325 mesh size, and zirconium powder from Strem Chemicals, Inc. with a 99.5% purity and a mesh size of -50. The rest of the secondary elements (silicon, zinc, magnesium, and zirconium) were chosen based upon their Moh's hardness values compared to both aluminum's and magnesium's: aluminum has a hardness of 2.75MPa, magnesium has a hardness of 2.5MPa,

silicon has a hardness of 6.5MPa, zinc has a hardness of 2.5MPa, and Zirconium has a hardness of 5MPa.

2.2. Characterization – X-ray Diffraction

After MA or MM, powders can be characterized for their microstructural features, phase constitution, shape, surface area, and size. It is particularly important to measure the grain size and the lattice strain within mechanically alloyed powders because transformation characteristics and phase constitution are critically dependent upon them [17]. X-ray Powder Diffraction (XRD) is a considerably powerful characterization technique for crystalline powders – it is an analytical technique that can be used for phase identification of crystalline material, it can provide unit cell dimensions through the use of/deviations from Bragg's Law, and it can be used to derive crystallite size and strain within metallic powders [47].

XRD peak broadening techniques are indicative of the elemental phases present, can help to evaluate the crystallite size of crystalline powders, and can also determine the lattice strain of the powder. Once a powder has undergone XRD, a plot of 2θ (θ referring to the angle in degrees) versus Intensity (which is typically represented as total counts or in counts per second) is generated and the pattern of peaks which is generated is a characteristic "fingerprint" of a certain phase. The positions of peaks in a powder pattern is determined by the shape, size, and symmetry of the phase's unit cell and the intensities depends upon the arrangement of atoms within the cell [78].

XRD for powder analysis does have its strengths and its limitations. XRD's strengths include: that it is powerful and rapid (depending upon the user's scanning preferences), it provides unambiguous phase determination in most cases, sample preparation is minimal, the

sample does not have to be discarded after undergoing XRD, and data interpretation is straight forward [47]. On the other hand: in order to determine an unknown, it is best to have a single phased and homogenous sample; one must have access to a standard reference of d-spacing's and 2θ angles, which can be hard to access and/or is relatively expensive; indexing non-isometric crystal systems is complicated; and peak overlay can occur, which worsens at higher angle "reflections" [47].

2.2.1. X-ray Diffraction Instrumentation – Rigaku Ultima III

For this research, a Rigaku Ultima III (as seen in Figure X), located within the Center for Functional Nanomaterials at Brookhaven National Laboratory, was used (Figure 12). Most X-ray diffractometers, including the Ultima III, consist of three basic elements: an X-ray tube, a sample holder, and an X-ray detector, which can be seen in Figure 13.

Figure 12: Rigaku Ultima III which was used for this research and is located at the Center for Functional Nanomaterials at Brookhaven National Laboratory in Upton, NY.

Figure 13: The Rigaku Ultima III's X-ray tube (A), sample holder (B), and an X-ray detector (C).

In the Rigaku Ultima III, X-rays are generated in a cathode ray tube by heating a filament to produce electrons, accelerating them towards a target by applying a voltage potential, and hitting the target with electrons [47]. When electrons have a high enough energy to dislodge inner shell electrons of the target, characteristic X-rays are produced. There are several different components which make up all of the characteristic X-rays that are produced, the most common of which being: Kα (which consists of $K\alpha_1$ and $K\alpha_2$) and Kβ [47]. $K\alpha_1$ has a wavelength which is roughly twice the intensity of $K\alpha_2$, and a slightly shorter wavelength than $K\alpha_2$; the specific wavelength and intensity of these X-rays are characteristic of the target material, and when using the Ultima III, the target material is copper [47]. Foils or crystal monochrometers then filter the characteristic X-rays in order to produce monochromatic rays that are required for XRD ($K\alpha_1$ and $K\alpha_2$ typically are close enough in wavelength where a weighted average of both is used) [47]. CuKα radiation's wavelength, λ, is 0.154184nm [47]. Lastly, the X-rays are collimated

and are then directed to the sample. As the sample and detector are rotating, the intensity of the X-rays that are reflected are recorded with respect to the angle. When the incident rays hit the sample and constructive interference occurs, it causes a peak in intensity [47]. The detector records the incoming X-ray signal at each angle increment, converts it to a count rate, and then sends it to a computer. The X-ray generator rotates at an angle θ across the sample while the X-ray detector rotates at an angle 2θ across the sample. A goniometer is used to maintain the angle and rotate the sample. After obtaining the data, data analysis can be performed with various computer programs, including Jade.

2.2.2. X-ray Powder Diffraction Fundamentals

When the incident, monochromatic X-rays interact with the powder sample, it produces constructive interference and a diffracted X-ray and when this occurs, it satisfies Bragg's Law [47]. Bragg's Law is the fundamental principle behind XRD – it relates the wavelength of the electromagnetic radiation (X-rays, in this case) to the diffracting beam's angle and then the lattice spacing within a crystalline sample [47]. The d-spacing of each phase present can be derived from Bragg's Law. Bragg's Law is:

$$n\lambda = 2d \sin\theta$$

where n is an integer (when n is a positive integer, constructive interference occurs), λ is the wavelength of the rays, θ is the angle between the incident rays and the crystal's surface, and d is the interatomic spacing between layers of atoms.

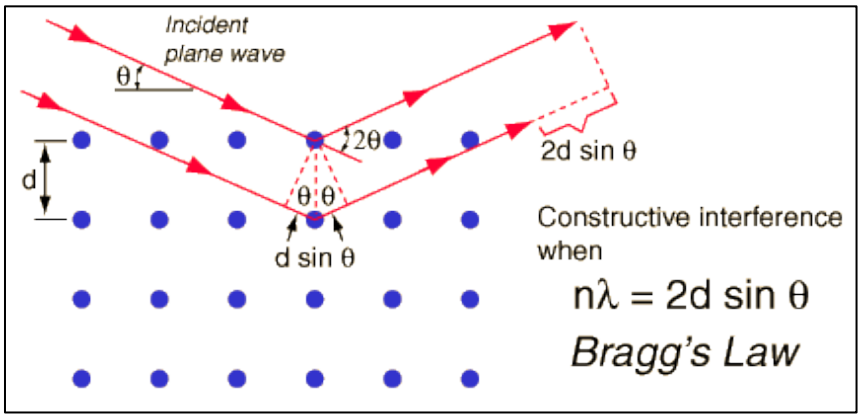

Figure 14: Schematic representation of Bragg's Law ($n\lambda = 2d\sin(\theta)$) during XRD [49].

While Bragg's Law is used for determining the d-spacing of a particular phase, there is more information about a sample that can be extracted from the peak's shape. The width of the peak can provide information about crystallite size and strain. XRD peaks are broadened due to small particle sizes, lattice strain within the material and instrumental effects [17]. Interestingly, instrumental effects play a big role in terms of dictating shape, as seen in Figure 15:

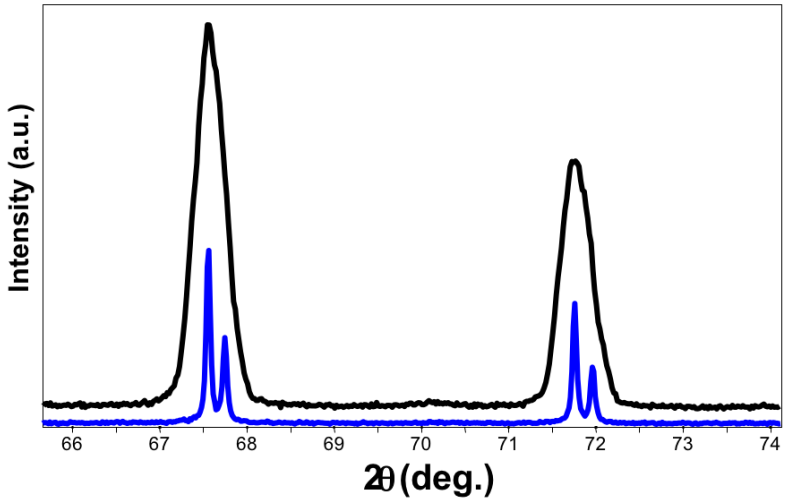

Figure 15: Diffraction patterns of silicon that were produced from the exact same sample, but with two different diffractometers that had different optical configurations [50]. This apparent peak broadening is due to instrumentation alone.

Once the effects of instrumentation are removed via estimation techniques used in computer software, during XRD pattern software analysis, crystallite size and lattice strain for the powder sample can be determined, which as stated earlier, is crucial for understanding how effective the MA process was and the state of the alloyed powder.

G.K. Williamson and his student, W.H. Hall were able to calculate the mean size of the crystallites and the strain within a powder independently from one another for the first time in 1953 [51]. The approximate formulas for β_L, or size broadening which was derived from the Scherrer equation, and β_e, or strain broadening, do vary differently with respect to the Bragg angle, θ:

$$\boldsymbol{\beta_L = \frac{K\lambda}{L\cos\theta}} \quad ; \quad \boldsymbol{\beta_e = C\varepsilon\tan\theta} \quad [36]$$

Where β_L is the broadening due to crystallite size (relating to the volume average), β_e is the broadening due to strain, L is the crystallite size, λ is the wavelength, **K** is the Scherrer constant, ε is the inhomogenous strain, and **C** is a constant that is dependent upon assumptions made about the inhomogenous strain (and typically equals either 4 or 5) [51].

If both contributions are present in the width of the peaks, then one can conclude that their combined effect should be determined by convolution [51]. If the sum of squares method for convolution is used in order to simplify the Williamson-Hall method, then:

$$\boldsymbol{\beta_{total} = \beta_L + \beta_e = C\varepsilon\tan\theta + \frac{K\lambda}{L\cos\theta}} \quad [51]$$

The equation of a line can be achieved by multiplying the equation above by $\cos(\theta)$:

$$\boldsymbol{\beta_{total}\cos\theta = C\varepsilon\sin\theta + \frac{K\lambda}{L}} \quad [51]$$

When comparing this to $y = mx + b$, one can see that by plotting β_{total}*cosθ versus sinθ, the strain component can be determined from the slope (**C**ε) and the crystallite size component from the intercept (**K**λ/L), which can also be seen in Figure 16:

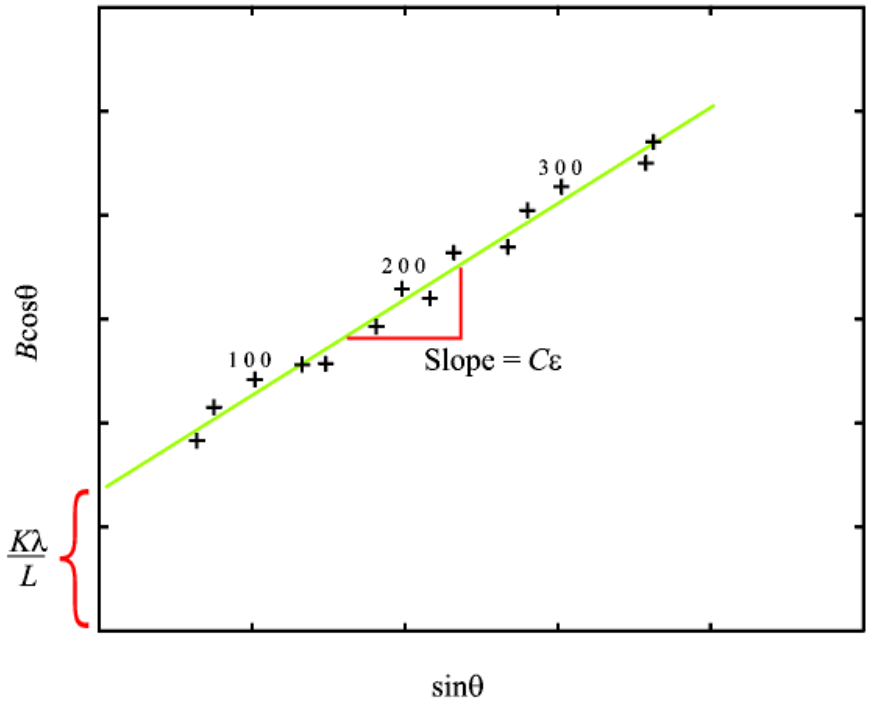

Figure 16: Williamson-Hall plot which can be used to derive the crystallite size and strain within powders by relating both contributions to peak widening by convolution (sum of squares) and getting the equation into the form "y = mx + b" [51].

Alternatively, the plot can also be expressed in reciprocal space parameters, β* and d*:

$$\boldsymbol{\beta^* = \frac{(FWHM_{radians})(\cos\theta_{radians})}{\lambda}} \quad ; \quad \boldsymbol{d^* = \frac{(2\sin\theta_{radians})}{\lambda}}$$

By using this form to create Williamson-Hall plots, either the information extracted from XRD analysis programs like Jade can be used to plot Williamson-Hall plots in Excel, and/or Williamson-Hall plots can be generated within the XRD analysis programs itself.

2.2.3. XRD Data Analysis – Jade

After the XRD data had been collected, it underwent data analysis using Jade, a software created by MDI. Jade is designed to peak profile fitting techniques in order to deliver accurate information about each peak to estimate crystallite size and strain [50]. This software empirically fits experimental data with a series of estimation techniques/equations which allows for precise peak positions, heights, areas, and widths with statistically valid estimates. Typically, diffraction peaks are a mixture of Gaussian or Lorentzian components, which is somewhat complicated [50]. So, the peaks are fit with either a Pseudo-Voigt (linear combination of Gaussian or Lorentzian components) or a Pearson VII (exponential mixture of Gaussian or Lorentzian components) curve [50]. After picking which function within the Profile Fitting section of Jade, the background function is then selected. Typically, the fixed or linear background function is used – both of these functions specify how the background underneath the peak will be modeled [50]. There are other functions which can be modified, but the most important are choosing which diffraction peak component computational method to use, along with how the computer should model the background. A typically data export file can be seen in Figure 17:

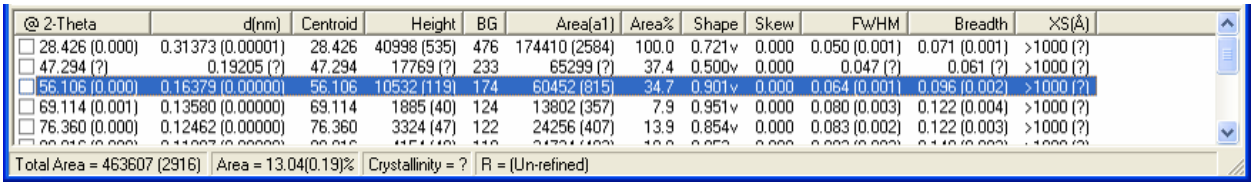

@ 2-Theta	d(nm)	Centroid	Height	BG	Area(a1)	Area%	Shape	Skew	FWHM	Breadth	XS(Å)
28.426 (0.000)	0.31373 (0.00001)	28.426	40998 (535)	476	174410 (2584)	100.0	0.721v	0.000	0.050 (0.001)	0.071 (0.001)	>1000 (?)
47.294 (?)	0.19205 (?)	47.294	17769 (?)	233	65299 (?)	37.4	0.500v	0.000	0.047 (?)	0.061 (?)	>1000 (?)
56.106 (0.000)	0.16379 (0.00000)	56.106	10532 (119)	174	60452 (815)	34.7	0.901v	0.000	0.064 (0.001)	0.096 (0.002)	>1000 (?)
69.114 (0.001)	0.13580 (0.00000)	69.114	1885 (40)	124	13802 (357)	7.9	0.951v	0.000	0.080 (0.003)	0.122 (0.004)	>1000 (?)
76.360 (0.000)	0.12462 (0.00000)	76.360	3324 (47)	122	24256 (407)	13.9	0.854v	0.000	0.083 (0.002)	0.122 (0.003)	>1000 (?)

Total Area = 463607 (2916) | Area = 13.04(0.19)% | Crystallinity = ? | R = (Un-refined)

Figure 17: Data output file from the Peak Profile Fitting program on Jade [50].

2.3. Experimental Procedures and Chosen Parameters

Within the following section, general procedures for both ball milling and X-ray Powder Diffraction are discussed in detail and calculations needed to solve for ball milling parameters are also discussed. Additionally, specific parameters and/or values for certain parameters for both the mechanism and characterization techniques are described.

2.3.1. Ball Milling Procedure

The actual process of mechanically alloying starts by adding powders in the right proportion into the jar along with a grinding medium (usually steel or tungsten carbide). First, the density of the powder(s) that are to milled should be measured because the density of the powder is going to be different than a solid of the same composition of the powder. This can be done by taking several weight measurements of a graduated cylinder being filled by powder, recording the weight and the volume, and then determining the density of the powder and the standard deviation of the density. The multiple weights and volumes should be recorded in order to ensure that the calculated density is accurate.

As described in Section 1.2.1.6. Percent Empty Space in Jar, there has to be enough empty space in the jar in order for the impact forces of the grinding media to be exerted on the powder; it is necessary for there to be enough empty space for the media and the powder particles to move around [17]. The percentage of empty space necessary in the jar depends upon the manufacturer's recommendations. Generally, about one third to half of the jar space is left empty [17,45,46]. In the case where one third of the space in the jar should be empty, one third of the volume is typically powder and one third of the volume is typically media [45,46]. Based upon the calculated powder density, the powder mass required to fill one third of the jar volume

can be calculated. From there, the volume of the of the grinding media can be calculated based upon the chosen or ideal BPR by the following steps:

1. Multiply the calculated weight of the powder by the chosen BPR – this will be the grinding media's weight

2. Weight the grinding media on a scale until the approximate weight required has been achieved, then count the number of balls that were weighed out

3. Calculate the volume of the grinding media, where V_{total} (mL) is the total volume of the grinding media in milliliters, # balls is the number of balls that were counted out, and r is the radius of the grinding media:

$$\boldsymbol{V_{total}(mL) = (\#\, balls) * (^{4}/_{3})\pi r^{3}] * (0.001\, ^{mL}/_{mm})}$$

The powder volume plus the grinding media volume should allow for one third of the jar volume at minimum to remain empty, if not, then the BPR should be changed.

After determining the number of balls needed to mill the correct powder volume, then the procedure for each run within that particular powder system is as follows:

1. Weigh the grinding media before each new run. Divide the weight of the media by the BPR

2. Multiply each weight percent of each powder by the quotient of the grinding media weight and the BPR to get the total weight of each powder to be put in to the jar, record these numbers

3. Weigh out each powder to get approximately what was calculated in the last step, record these numbers
4. Add the percentage of PCA to the jar along with the weighed, clean media
5. Calculate the total mass of the jar, media, and powder together
6. Put sealed jar into ball mill properly, change the milling parameters if needed (milling speed, time, intervals, etc.)
    i. Ensure that the counter weight opposite the jar is accurate to total jar's weight (it is crucial that the jar's weight is balanced) – if it is not, the milling container should shut off and display an error message
7. Watch the ball mill for approximately ten minutes to ensure that the ball mill is functioning properly
8. After run has been completed and the jar has sufficiently cooled down (which should take around one to two hours), the powder is collected off of the grinding media and the gar as much as possible, the jar is cleaned thoroughly with either methanol or ethanol with Kimtech Kimwipes (or some other low lint paper product), and the grinding media is cleaned with a sonicator for at least a half an hour

This procedure work will continue for a certain powder system as long as the desired powder volume and the BPR stays the same. If any of those two variables change, this entire procedure should be repeated (unless the powder density will not change, and in that event, that section

should be skipped). After the powder has been cleaned out of the milling jar, it undergoes characterization via X-ray Powder Diffraction.

2.3.2. Ball Milling – Chosen Parameters

Elemental aluminum, magnesium, silicon, zinc, and zirconium powders were milled in a Retsch PM100 Planetary Ball Mill to produce four different binary, nanocrystalline alloys consisting of 99 atomic % aluminum, and 1 atomic % either magnesium, silicon, zinc, or zirconium. The powders were acquired from the following: aluminum powder from Alfa Aesar with a 99.5% purity and a mesh size of -325, magnesium powder from Alfa Aesar with a 99.8% purity and a mesh size of -325, silicon powder from Alfa Aesar with a 99.5% purity and a mesh size of 325, zinc powder from Alfa Aesar with a 99.9% purity and a -140 to 325 mesh size, and zirconium powder from Strem Chemicals, Inc. with a 99.5% purity and a mesh size of -50.

The ball milling procedure was followed from section 2.3.2. A 50mL tungsten carbide with 5mm tungsten carbide media was used for all runs. The ball mill was located in an argon filled glove box to ensure that the environment in which the ball mill is milling is controlled. The PCA was chosen to be 2% stearic acid, the BPR was 5:1, the milling speed was 550RPM, and there was no interval used during milling. Once the milling run was over, one to two hours was added to the time in order to allow the powder to sufficiently cool. Once the powder was collected, the jar and media were cleaned with methanol or ethanol, and then the media underwent sonication for a half an hour to ensure no powder particles contaminated the media's surfaces. Next, the powder underwent XRD analysis.

2.3.3. General X-ray Powder Diffraction Procedure

This procedure was followed during X-ray powder diffraction analysis:

1. The sample was prepared under a HEPA (High Efficiency Particulate Air) filtered hood – powder was placed into the sample holder with a uniform height and a smooth surface (if any clumps of powder were present, they were removed). The sample holders that were used can be seen in Figure 18:

Figure 18: Example of what the powder sample holder that was used throughout XRD analysis looks like [51].

2. The radiation was turned on (which increased the voltage to 20kV and the current to 2mA).

3. The "everyday use" macro was then turned on. This macro will slowly ramp up the voltage and current until they reach operating values: V = 40kV, I = 44mA, and the State = 1.76kW. Because this takes a few minutes, the goniometer undergoes initialization of all its axes at the same time.

4. After the "everyday use" macro runs and initialization is complete, the sample can then be put on the stage. At this time, the divergence height limiting slit (which is responsible for the controlling the horizontal divergence of X-rays, or in other words, the area of the sample experiencing irradiation) should be placed in the X-ray tube.

The largest divergence height limiting slit (10mm, or H10) is used, as seen in Figure 19:

Figure 19: The divergence height limiting slit used throughout XRD analysis. It is the largest slit that can be used; meaning that it allows for all of the sample be irradiated.

5. Next, the sample height and tilt is configured. 2θ/Ω is moved to 0, the attenuator (which is used to reduce the intensity of the beam) is moved from open to 1/800, and then the only three variable slits within the goniometer are moved as follows: the divergence slit (DS) is moved to 0.1mm, the scattering slit (SS) is moved to 1mm, and the receiving slit (RS) is moved to 0.1mm. A schematic of the goniometer's layout can be seen in Figure 20:

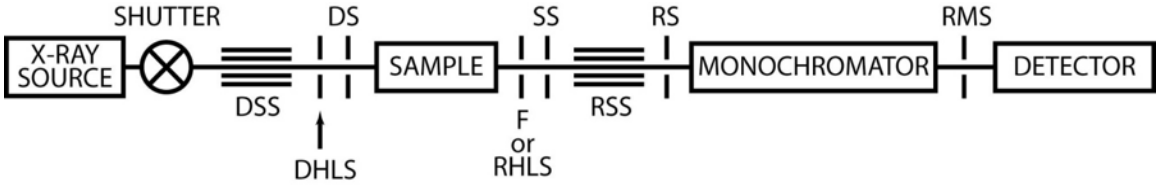

Figure 20: Schematic of the goniometer's layout [51]. The only variable slits that are adjusted are DS (divergence slit), SS (scattering slit), and RS (receiving slit). The rest are either fixed or are adjusted automatically by computer software.

6. A rough Z scan is performed from -2.5mm to -0.5mm, with a speed of 5mm/min, and a sample width of 0.1. An S-curve should be generated as seen in Figure 21. A spot

was chosen in the middle of the curve, then Z was moved to that position. The first Z measurement was recorded in a laboratory notebook.

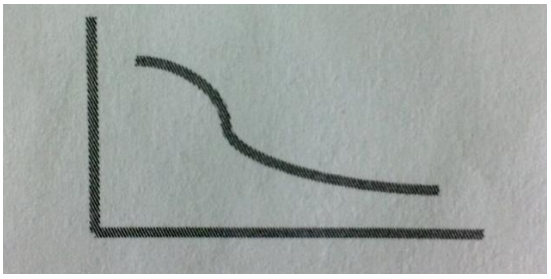

Figure 21: Approximate shape of S-curve which is generated during the initial Z scan.

7. Ry is then measured. It is measured between -1 and 1 degrees, with a width of 0.1, and a speed of 2. The resulting curve is in the shape of a positive parabola. The top of the parabola is determined and then Ry is moved to that location. The Ry measurement was recorded in a laboratory notebook.

8. A second Z scan is performed in order to determine that the ideal Z position did not change due to the change in Ry. The range at which this Z scan is performed was based upon the results of the first Z scan (for instance, if the results of the first Z scan were -1.8, choosing -2.0 to -1.6 is reasonable). The sample width is now 0.001, and the speed is 0.5. The curve generated is similar to that seen in Figure A, and point in the middle of the curve is where Z should be moved to. The second Z measurement was recorded in a laboratory notebook.

9. Now the parameters for the final scan are being set up in these last steps. First, the divergence slit and the receiving slit are moved to 0.2mm (the scattering slit was kept

at 1mm). Then, the attenuator was moved from 1/800 to open. Lastly, the 2θ/Ω under goes a quick, continuous scan in order to make sure that the first peak that was expected is present. For instance, aluminum (111), or aluminum's first peak, occurs at a 2θ measurement of approximately 38.472°. So, a rough, continuous scan of the sample was selected to run from 33° - 43°, with a step size (or width) of 0.1, and a speed of 5 degrees/minute. The first peak should appear, and the angle at which it occurs is recorded in a laboratory notebook.

10. The final run is now to be set up. The degree range should be chosen based upon known peaks of the phases and/or elements that are expected to be seen. The final scan was performed with the FT (fixed time) method, with a degree range which suited the sample's constituents, with a step size (w) of 0.1, a count time that allowed the user to maximize the allotted time they had scheduled with the machine (the angle range, or Δ angle, divided by the step size (w) gives the number of steps (# steps); the number of steps multiplied by the count time (CT) and divided by 3600 seconds per hour gives the approximate run time in hours as shown below), and the counting unit was chosen to be CPS, or counts per second.

$$\boldsymbol{\Delta\, angle}_{/\boldsymbol{w}} = \boldsymbol{\#\, steps} \quad ; \quad \frac{\boldsymbol{\#\, steps} * \boldsymbol{CT}}{\boldsymbol{3600}\left({}^{\boldsymbol{s}}/_{\boldsymbol{hr}}\right)} = \boldsymbol{Run\, Time}\ (\boldsymbol{hrs})$$

Once the run had been completed, the raw data was saved, the sample was removed from the diffractometer, and the diffractometer was shut down properly.

2.3.4. X-ray Powder Diffraction – Chosen Parameters

The XRD procedure is followed exactly from section 2.3.3. For nearly every XRD session, the specified count time allowed for approximately 4 or more hours of analysis.

After the XRD analysis has been completed, Jade is used for data analysis. By using Jade's peak profile fitting tool, the Pearson VII and Pseudo-Voigt estimation techniques for best peak fitting are selected in order to extract the information seen in Figure 15 from the peaks. Afterwards, graphs of the 2theta/omega versus intensity peaks are generated and Williamson Hall Plots are made in Excel to calculate crystallite size/grain size and strain. A table of of d_{hkl} measurements for each characteristic 2θ peak for each element that is being used in this thesis work can be seen in Table 4 and the unmilled, pure aluminum peaks can be seen in Figure 22.

Table 4: List of d_{hkl} measurements for each characteristic 2θ peak for each element that is being used in this thesis work [53].

Aluminum		Magnesium		Silicon		Zinc		Zirconium	
d_{hkl}	2θ (°)	d_{hkl}	2θ (°)	d_{hkl}	2θ (°)	d_{hkl}	2θ (°)	d_{hkl}	2θ (°)
(111)	38.472	(100)	32.178	(111)	28.443	(002)	36.291	(100)	31.948
(200)	44.720	(002)	34.395	(220)	47.304	(100)	38.996	(002)	34.847
(220)	65.095	(101)	36.612	(113)	56.124	(101)	43.223	(101)	36.515
(113)	78.228	(102)	47.813	(222)	58.858	(102)	54.323	(102)	47.993
(222)	82.434	(110)	57.371	(400)	69.132	(103)	70.078	(110)	56.935
		(103)	63.063	(331)	76.378	(110)	70.636	(103)	63.572
		(200)	67.319	(420)	78.739	(004)	77.051	(200)	66.789
		(112)	68.632	(224)	88.032	(112)	82.092	(112)	68.514
		(201)	70.008			(200)	83.756	(201)	69.556
		(004)	72.504			(201)	86.545	(004)	73.576
		(202)	77.833			(104)	89.927	(202)	77.596
		(104)	81.545					(104)	82.457

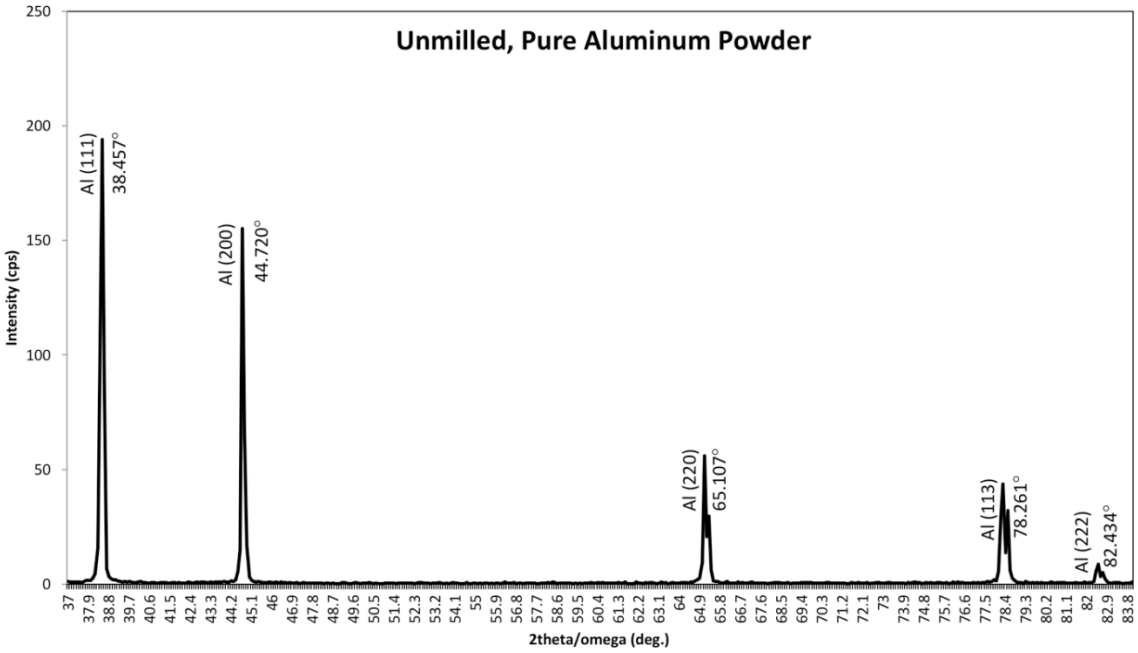

Figure 22: XRD peaks of pure, unmilled aluminum powder. The sample was scanned from 37°-84°, the grain size was calculated to be 83.333nm and the strain was calculated to be 0.00015.

Chapter 3: Synthesis of Results and Discussion

3.1. Aluminum – Silicon Alloys

99 atomic % aluminum and 1 atomic % silicon were milled for 1 hour, 4 hours, 8 hours, and 16 hours at a powder volume of 16.5mL, and an additional 8 hour run was completed using only a powder volume of 8mL. Because silicon has a much higher hardness than aluminum – 6.5MPa versus 2.75MPa – silicon is not expected to chemically mix with aluminum.

Results from these powder runs can be seen in Figure 23 through Figure 29.

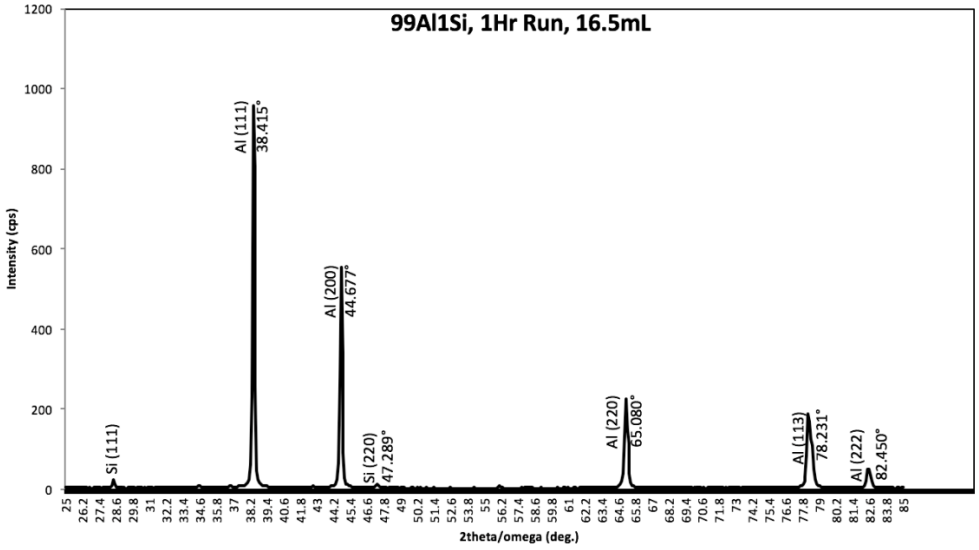

Figure 23: 99 atomic % aluminum, 1 atomic % silicon milled for 1 hour with 2% SA and a 5:1 BPR. To produce a volume of approximately 16.5mL of powder, 21.366g of aluminum powder and 0.225g of silicon powder. The resulting powder underwent XRD from 25°-85° with a count time (CT) of 70. Peaks that are present without an angle given to them are angles that Jade software did not pick up with either the Pearson VII or Pseudo-Voight approximations. The grain size was calculated to be 97.087nm and the strain was calculated to be 0.0006. Because there are peaks of silicon still present, this system has not chemically mixed.

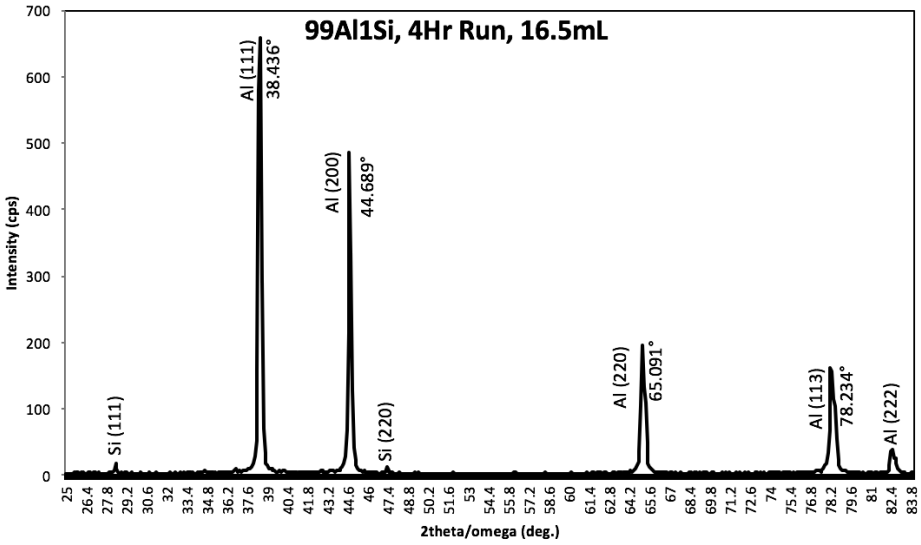

Figure 24: 99 atomic % aluminum, 1 atomic % silicon milled for 4 hours with 2% SA and a 5:1 BPR. To produce a volume of approximately 16.5mL of powder, 21.360g of aluminum powder and 0.224g of silicon powder. The resulting powder underwent XRD from 25°-85° with a count time (CT) of 17. Peaks that are present without an angle given to them are angles that Jade software did not pick up with either the Pearson VII or Pseudo-Voight approximations. The grain size was calculated to be 63.291nm and the strain was calculated to be 0.0003. Because there are peaks of silicon still present, this system has not chemically mixed.

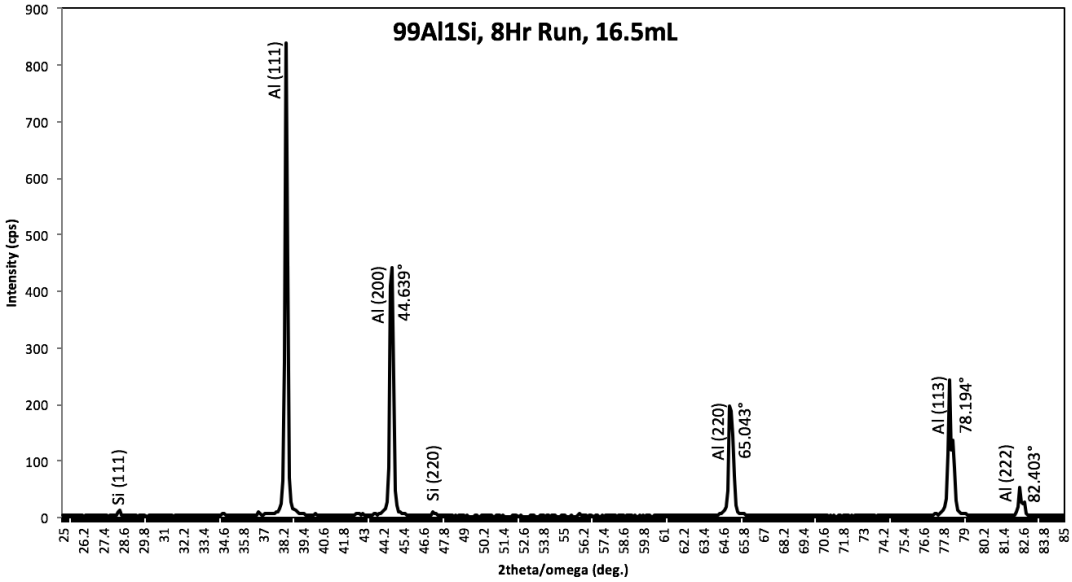

Figure 25: 99 atomic % aluminum, 1 atomic % silicon milled for 8 hours with 2% SA and a 5:1 BPR. To produce a volume of approximately 16.5mL of powder, 21.357g of aluminum powder and 0.224g of silicon powder. The resulting powder underwent XRD from 25°-85° with a count time (CT) of 20. Peaks that are present without an angle given to them are angles that Jade software did not pick up with either the Pearson VII or Pseudo-Voight approximations. The grain size was calculated to be 45.045nm and the strain was calculated to be 0.00055. Because there are peaks of silicon still present, this system has not chemically mixed.

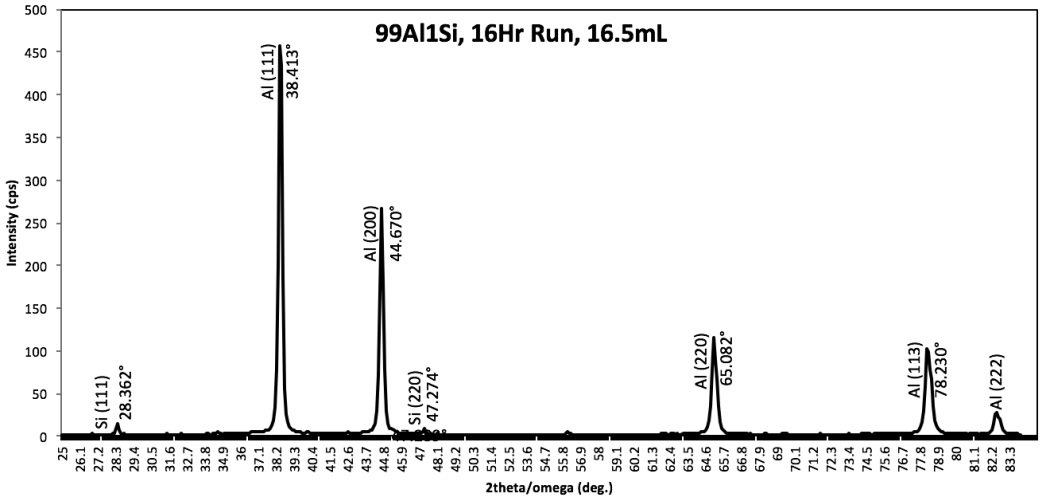

Figure 26: 99 atomic % aluminum, 1 atomic % silicon milled for 16 hours with 2% SA and a 5:1 BPR. To produce a volume of approximately 16.5mL of powder, 21.403g of aluminum powder and 0.224g of silicon powder. The resulting powder underwent XRD from 25°-85° with a count time (CT) of 70. Peaks that are present without an angle given to them are angles that Jade software did not pick up with either the Pearson VII or Pseudo-Voight approximations. The grain size was calculated to be 74.074 and the strain was calculated to be 0.0008. Because there are peaks of silicon still present, this system has not chemically mixed.

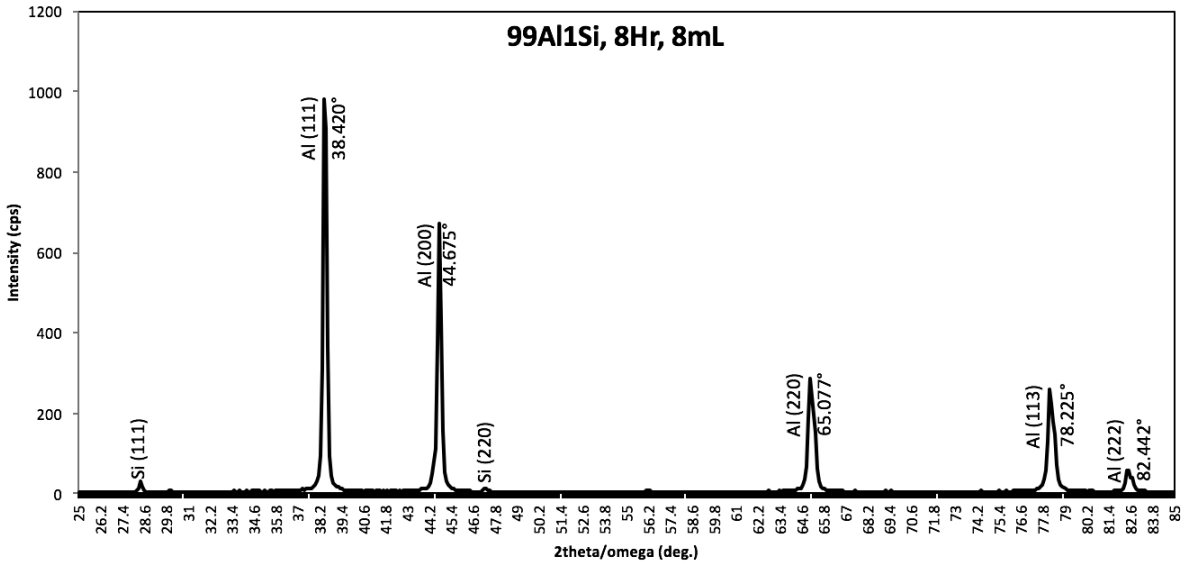

Figure 27: 99 atomic % aluminum, 1 atomic % silicon milled for 8 hours with 2% SA and a 5:1 BPR. To produce a volume of approximately 8mL of powder, 10.393g of aluminum powder and 0.1g of silicon powder. The resulting powder underwent XRD from 25°-85° with a count time (CT) of 24. Peaks that are present without an angle given to them are angles that Jade software did not pick up with either the Pearson VII or Pseudo-Voight approximations. The grain size was calculated to be 60.241nm and the strain was calculated to be 0.0003. Because there are peaks of silicon still present, this system has not chemically mixed.

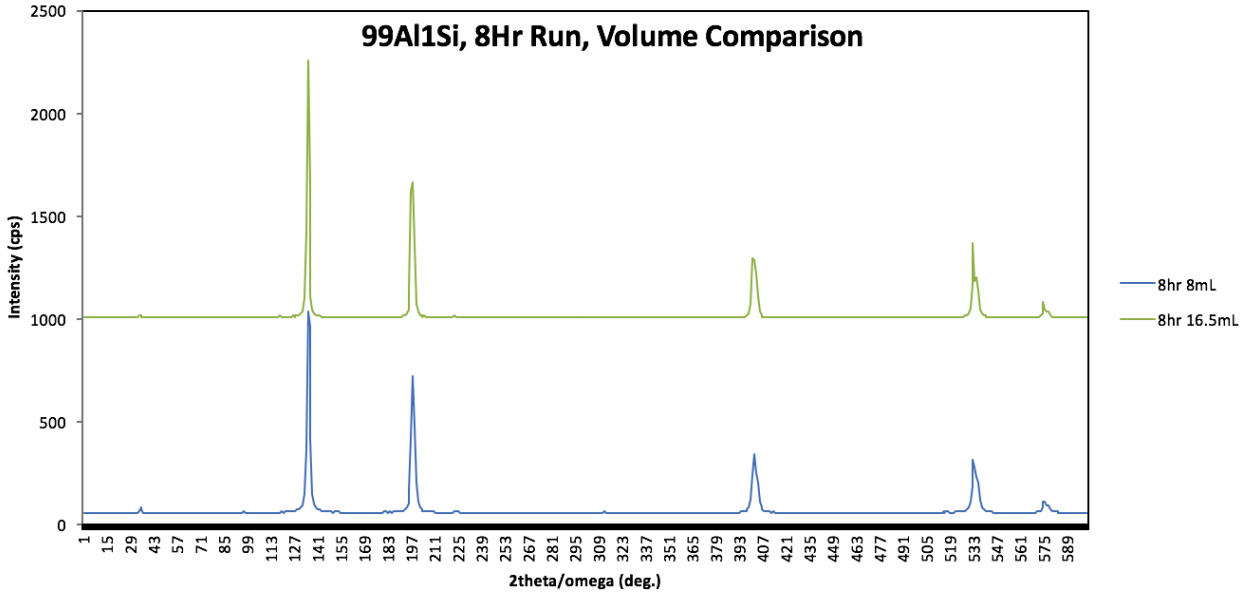

Figure 28: 99Al1Si peaks after an 8Hr run with 8mL of powder and an 8Hr run with 16.5mL of powder. The difference in peak width is minimal, the 16.5mL run had a smaller grain size, and the 8mL run had the smaller strain. Increasing the empty jar volume did not encourage chemical mixing like the aluminum-magnesium alloy system.

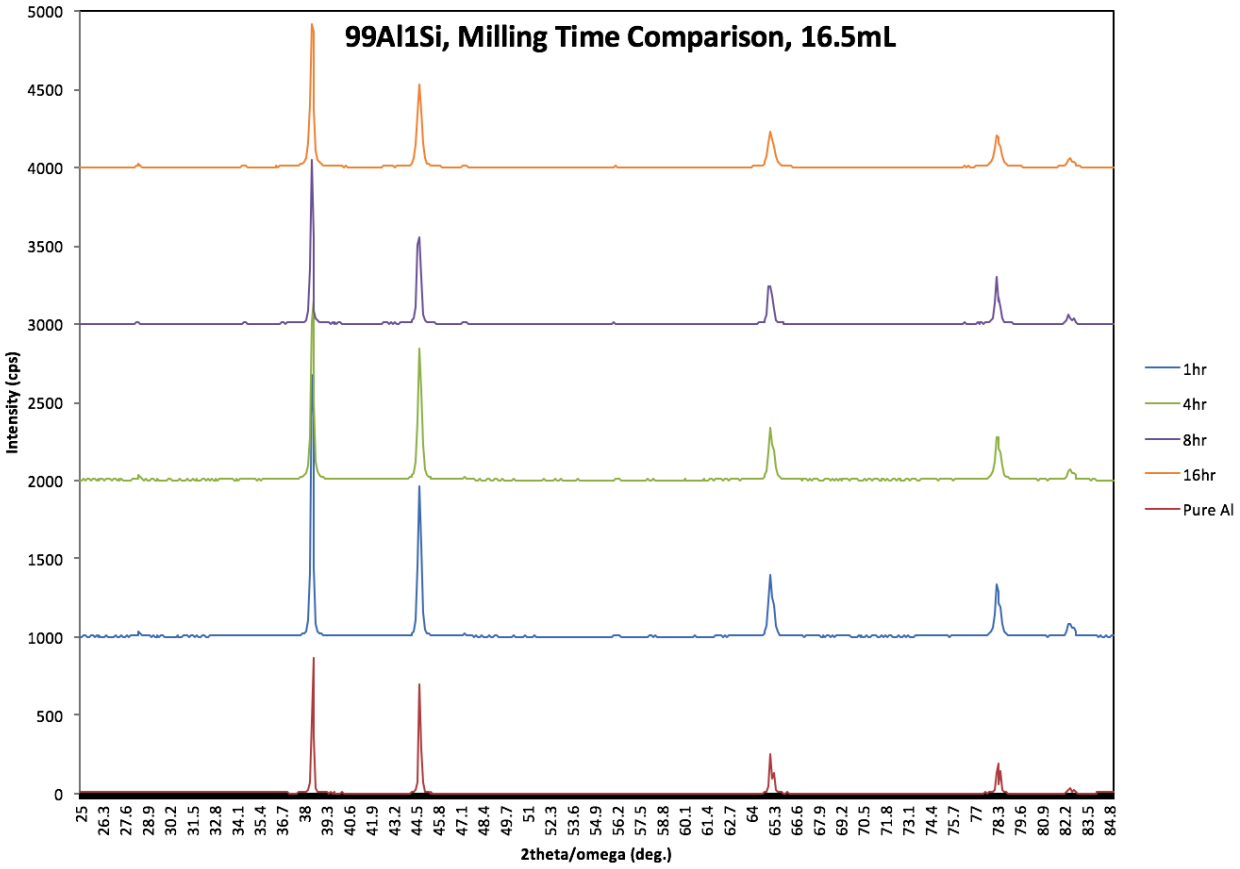

Figure 29: 99Al1Si milling time comparison for 16.5mL runs. The difference between the 99Al1Si peaks are minimal and this is to be expected because silicon has a much higher hardness (6.5MPa) than aluminum (2.75MPa) – making it hard for this mixture to chemically mix. There seems to be no reduction in the silicon peak, so the likelihood of this system chemically mixing seems very unlikely.

3.2. Aluminum – Zinc Alloys

99 atomic % aluminum and 1 atomic % zinc were milled for 1 hour, 4 hours, 8 hours, and 16 hours at a powder volume of 16.5mL, and an additional 8 hour run was completed using only a powder volume of 8mL. Because zinc's hardness is slightly less than aluminum's – 2.5MPa versus 2.75MPa – the likelihood of this powder system chemically mixing compared to the aluminum-silicon system is greater; however, the XRD peaks show that zinc did not chemically mix with aluminum in all figures besides the 1Hr, 16.5mL run.

Results from these powder runs can be seen in Figure 30 through Figure 35.

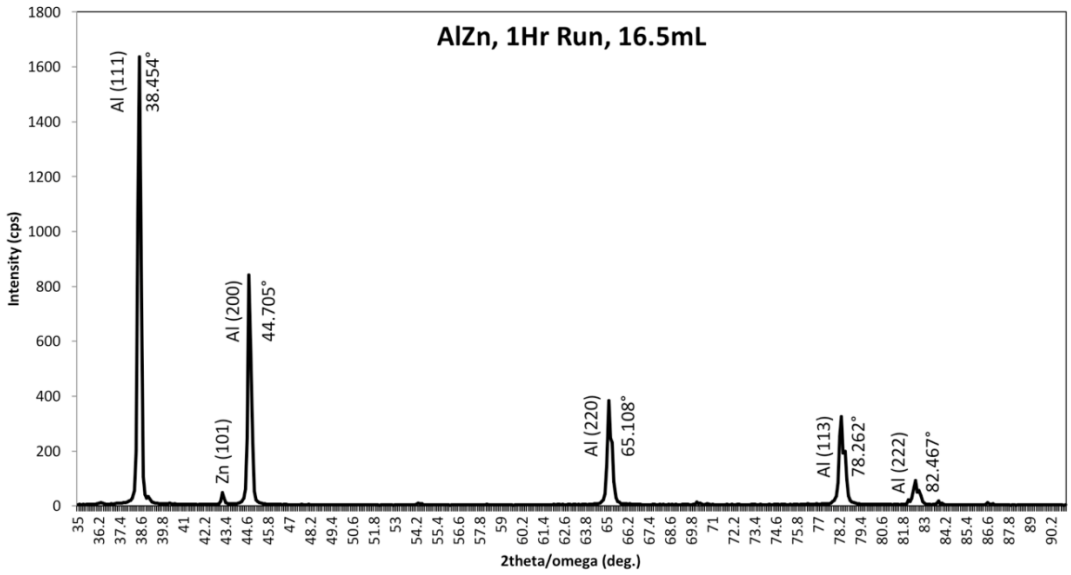

Figure 30: 99 atomic % aluminum, 1 atomic % zinc milled for 1 hour with 2% SA and a 5:1 BPR. To produce a volume of approximately 16.5mL of powder, 21.069g of aluminum powder and 0.5g of zinc powder. The resulting powder underwent XRD from 35°-91° with a count time (CT) of 21. Peaks that are present without an angle given to them are angles that Jade software did not pick up with either the Pearson VII or Pseudo-Voight approximations. The grain size was calculated to be 59.880nm and the strain was calculated to be 0.00003. Because there are peaks of zinc still present, this system has not chemically mixed.

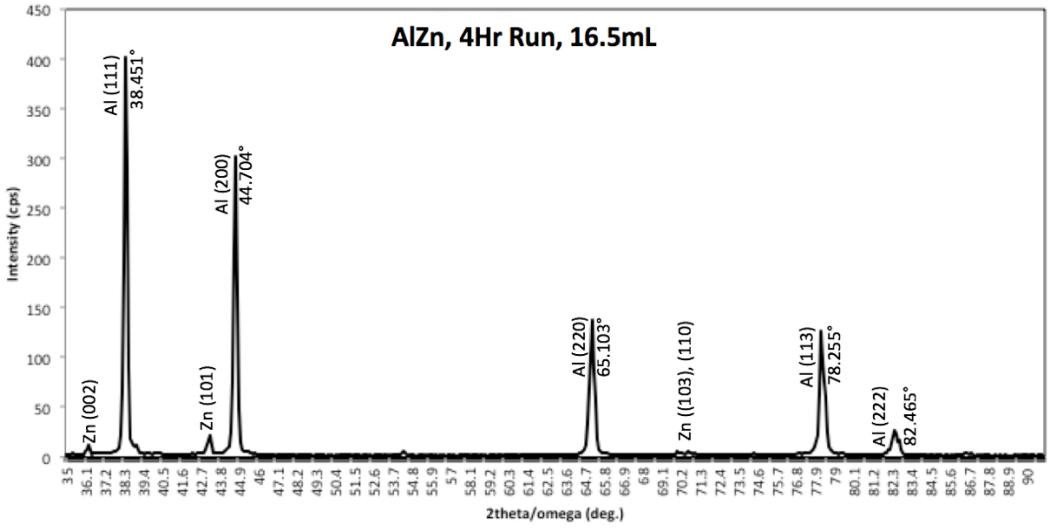

Figure 31: 99 atomic % aluminum, 1 atomic % zinc milled for 4 hours with 2% SA and a 5:1 BPR. To produce a volume of approximately 16.5mL of powder, 21.089g of aluminum powder and 0.5g of zinc powder. The resulting powder underwent XRD from 35°-91° with a count time (CT) of 22. Peaks that are present without an angle given to them are angles that Jade software did not pick up with either the Pearson VII or Pseudo-Voight approximations. The grain size was calculated to be 83.333nm and the strain was calculated to be 0.00015. Because there are peaks of zinc still present, this system has not chemically mixed.

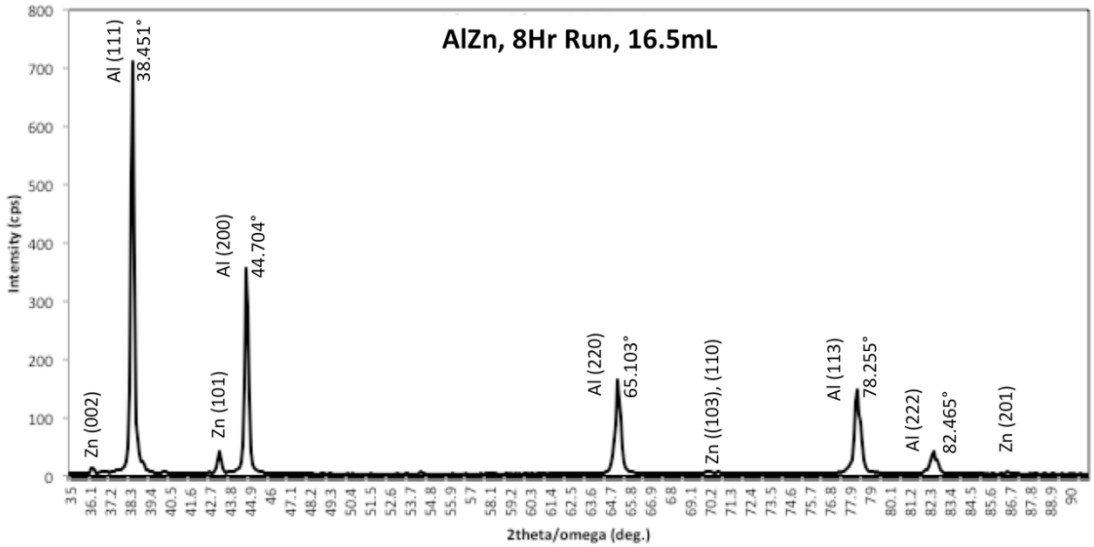

Figure 32: 99 atomic % aluminum, 1 atomic % zinc milled for 8 hours with 2% SA and a 5:1 BPR. To produce a volume of approximately 16.5mL of powder, 21.08g of aluminum powder and 0.5g of zinc powder. The resulting powder underwent XRD from 35°-91° with a count time (CT) of 74. Peaks that are present without an angle given to them are angles that Jade software did not pick up with either the Pearson VII or Pseudo-Voight approximations. The grain size was calculated to be 52.083nm and the strain was calculated to be 0.00015. Because there are peaks of zinc still present, this system has not chemically mixed.

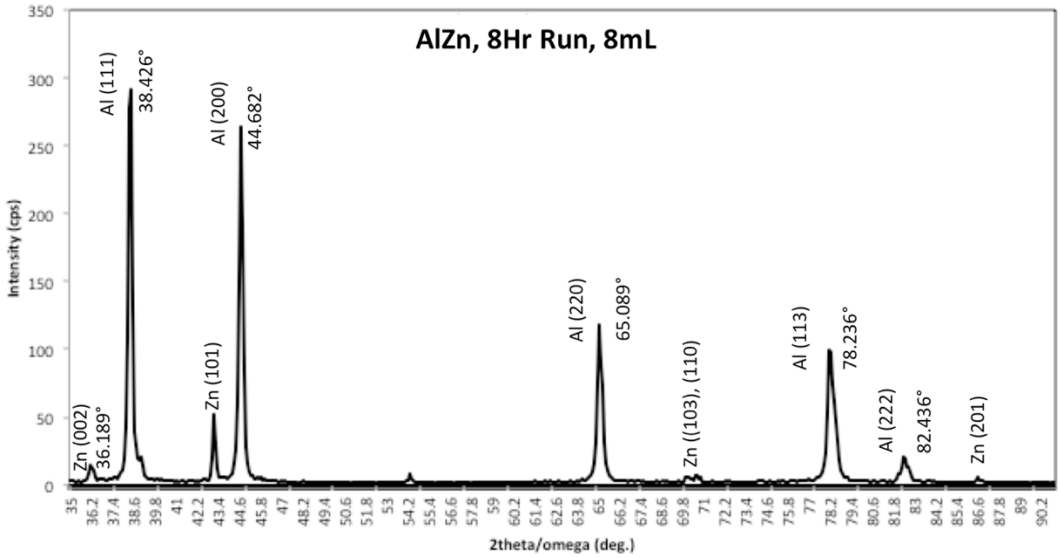

Figure 33: 99 atomic % aluminum, 1 atomic % zinc milled for 8 hours with 2% SA and a 5:1 BPR. To produce a volume of approximately 8mL of powder, 10.178g of aluminum powder and 0.2g of zinc powder. The resulting powder underwent XRD from 35°-91° with a count time (CT) of 22. Peaks that are present without an angle given to them are angles that Jade software did not pick up with either the Pearson VII or Pseudo-Voight approximations. The grain size was calculated to be 45.249nm and the strain was calculated to be 0.00001. Because there are peaks of zinc still present, this system has not chemically mixed.

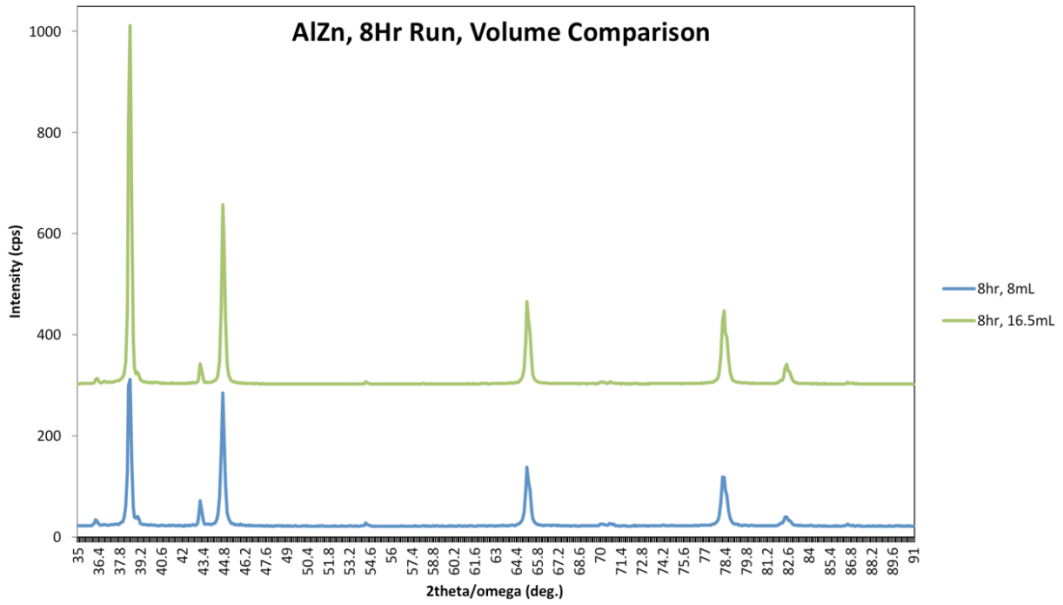

Figure 34: 99Al1Zn peaks after an 8Hr run with 8mL of powder and an 8Hr run with 16.5mL of powder. The difference in peak width is minimal; however, the 8mL run had the smaller grain size and had less strain. Increasing the empty jar volume did not encourage chemical mixing like the aluminum – magnesium system.

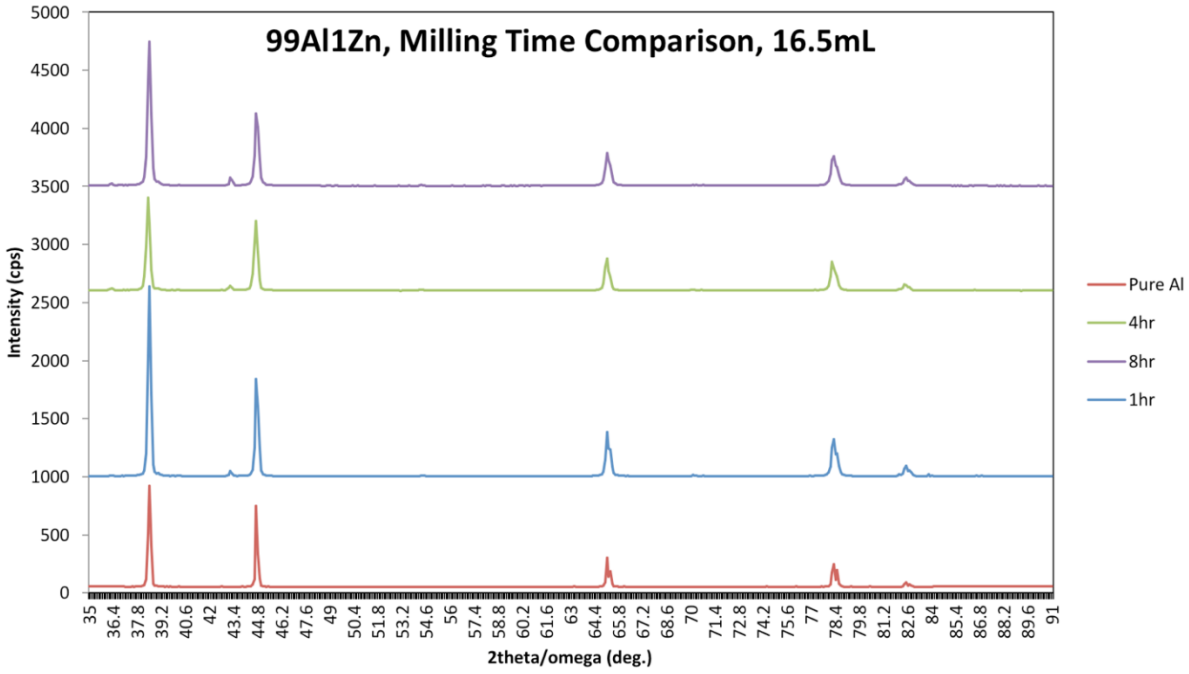

Figure 35: 99Al1Zn milling time comparison for 16.5mL runs. The Zn peaks became more defined as the milling time increased, which is interesting because zinc's hardness is slightly less than aluminum's – 2.5MPa versus 2.75MPa – the likelihood of this powder system chemically mixing compared to the aluminum-silicon system is greater. There seems to be no reduction in the zinc peak, so the likelihood of this system chemically mixing seems very unlikely.

3.3. Aluminum – Magnesium Alloys

99 atomic % aluminum and 1 atomic % magnesium were milled for 1 hour, 4 hours, and 8 hours at a powder volume of 8mL, and then for 1 hour, 4 hours, 8 hours, and 16 hours at a powder volume of 16.5mL. Because magnesium's hardness is slightly less than aluminum's – 2.5MPa versus 2.75MPa – the likelihood of this powder system chemically mixing compared to the aluminum-silicon system is greater. This powder system did chemically mix, and it occurred in the 8Hr, 8mL run and the 16Hr, 16.5mL run. Interestingly, zinc's hardness is the same as magnesium's and unlike magnesium, aluminum and zinc did not chemically mix.

Results from these powder runs can be seen in Figure 36 through Figure 45.

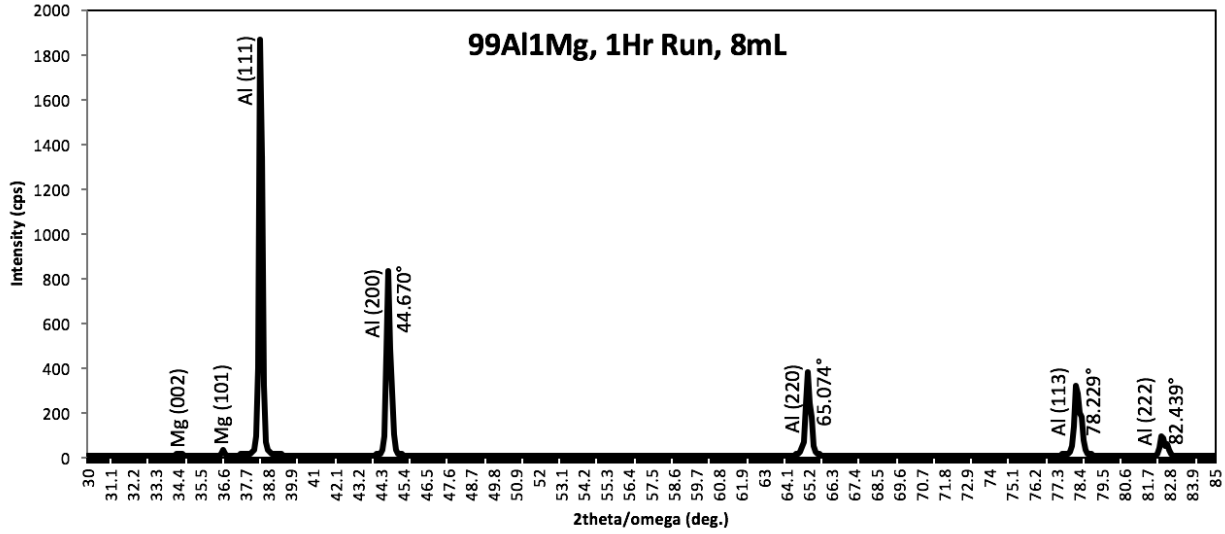

Figure 36: 99 atomic % aluminum, 1 atomic % magnesium milled for 1 hour with 2% SA and a 5:1 BPR. To produce a volume of approximately 8mL of powder, 10.3936g of aluminum powder and 0.1g of magnesium powder. The resulting powder underwent XRD from 30°-85° with a count time (CT) of 33. Peaks that are present without an angle given to them are angles that Jade software did not pick up with either the Pearson VII or Pseudo-Voight approximations. The grain size was calculated to be 56.497 and the strain was calculated to be 0.0001. Because there are peaks of magnesium still present, this system has not chemically mixed.

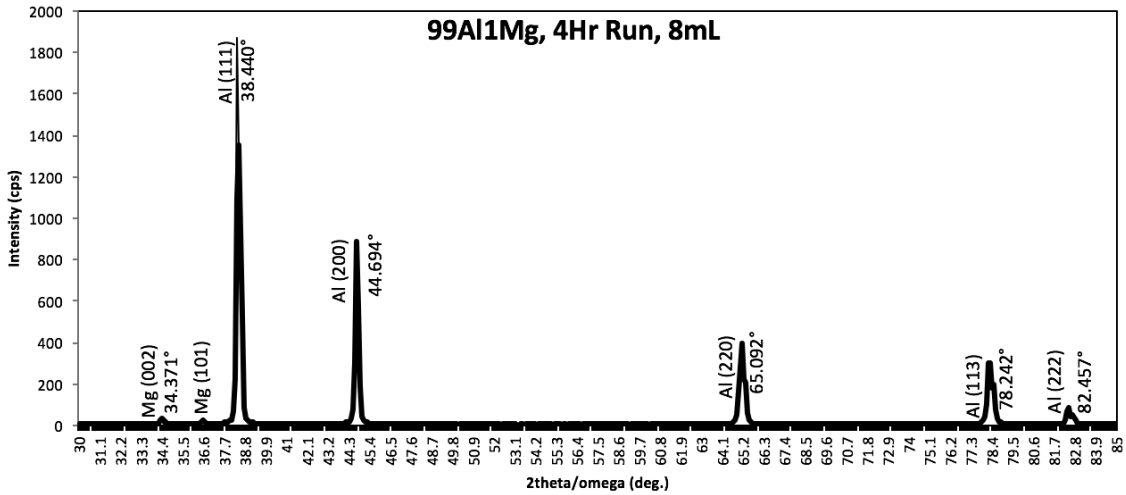

Figure 37: 99 atomic % aluminum, 1 atomic % magnesium milled for 4 hours with 2% SA and a 5:1 BPR. To produce a volume of approximately 8mL of powder, 10.342g of aluminum powder and 0.1g of magnesium powder. The resulting powder underwent XRD from 30°-85° with a count time (CT) of 67. Peaks that are present without an angle given to them are angles that Jade software did not pick up with either the Pearson VII or Pseudo-Voight approximations. The grain size was calculated to be 204.082nm and the strain was calculated to be 0.0007. Because there are peaks of magnesium still present, this system has not chemically mixed.

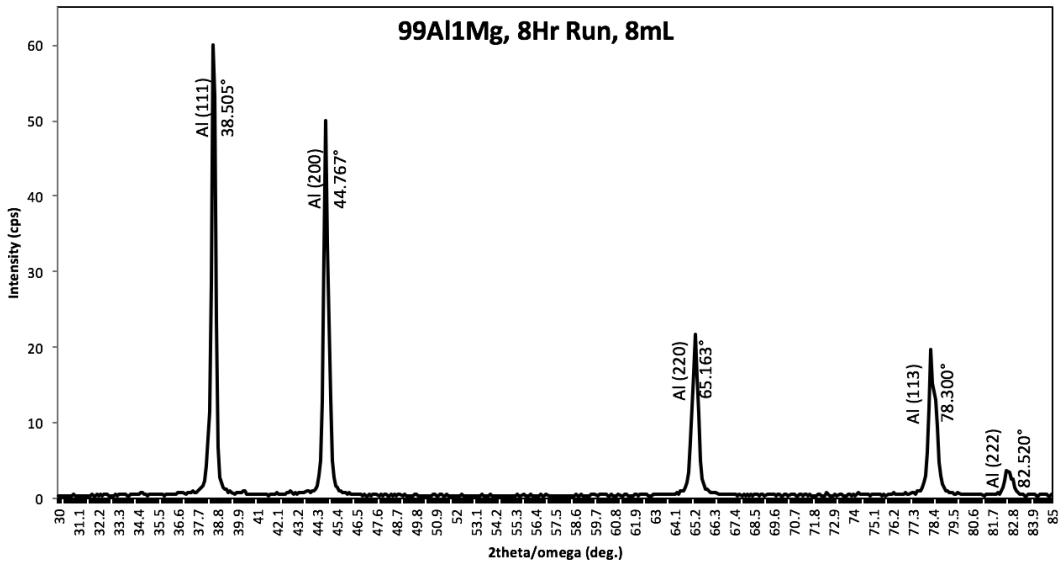

Figure 38: 99 atomic % aluminum, 1 atomic % magnesium milled for 8 hours with 2% SA and a 5:1 BPR. To produce a volume of approximately 8mL of powder, 10.337g of aluminum powder and 0.1g of magnesium powder. The resulting powder underwent XRD from 30°-85° with a count time (CT) of 95. Peaks that are present without an angle given to them are angles that Jade software did not pick up with either the Pearson VII or Pseudo-Voight approximations. The grain size was calculated to be 44.843nm and the strain was calculated to be 0.00015. Because there are no peaks of magnesium present, this system has chemically mixed.

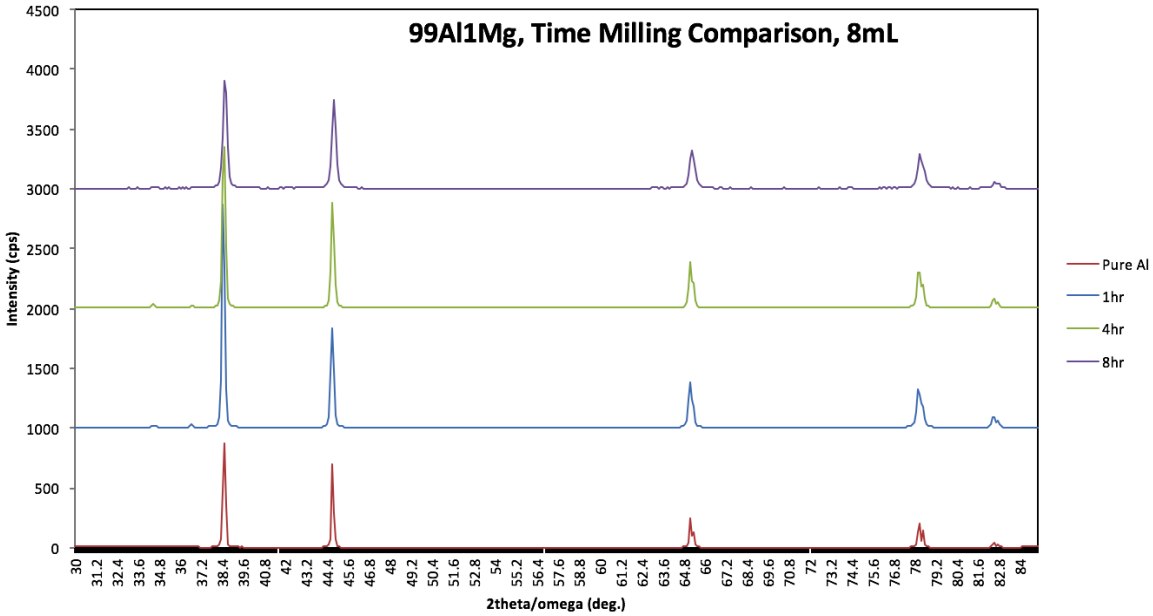

Figure 39: 99Al1Mg milling time comparison for 8mL runs. The magnesium peaks disappeared as the milling time increased, which proves that magnesium and aluminum did mix, like Murdoch and Schuh's thermodynamic model had suggested and S.M. Umbraikar et al. experimentally had proven [10,11]. There is a reduction of the magnesium peaks over time, so this system can be milled till it chemically mixed.

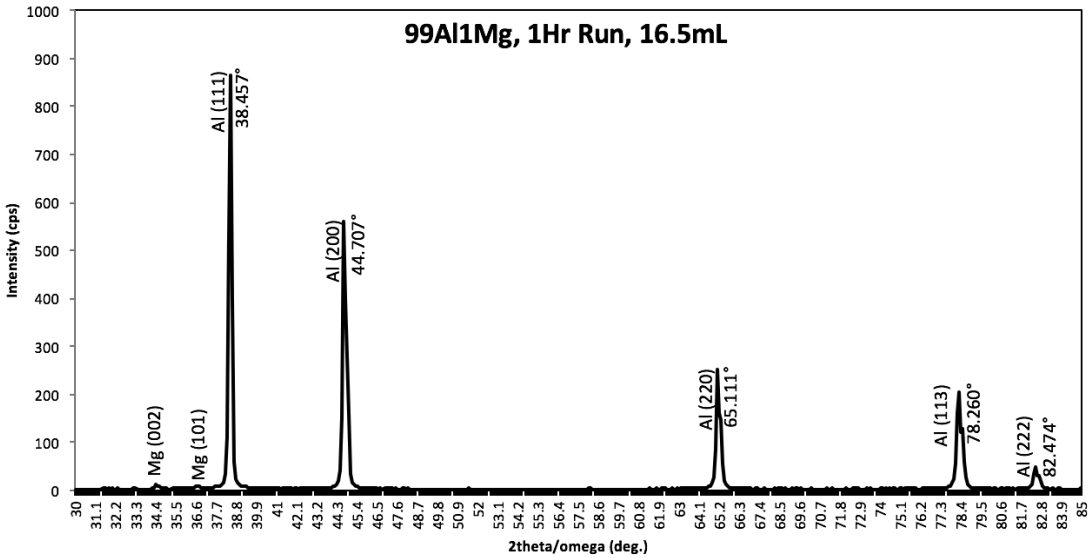

Figure 40: 99 atomic % aluminum, 1 atomic % magnesium milled for 4 hours with 2% SA and a 5:1 BPR. To produce a volume of approximately 16.5mL of powder, 21.4g of aluminum powder and 0.2g of magnesium powder. The resulting powder underwent XRD from 30°-85° with a count time (CT) of 23. Peaks that are present without an angle given to them are angles that Jade software did not pick up with either the Pearson VII or Pseudo-Voight approximations. The grain size was calculated to be 74.074nm and the strain was calculated to be 0.00025. Because there are peaks of magnesium still present, this system has not chemically mixed.

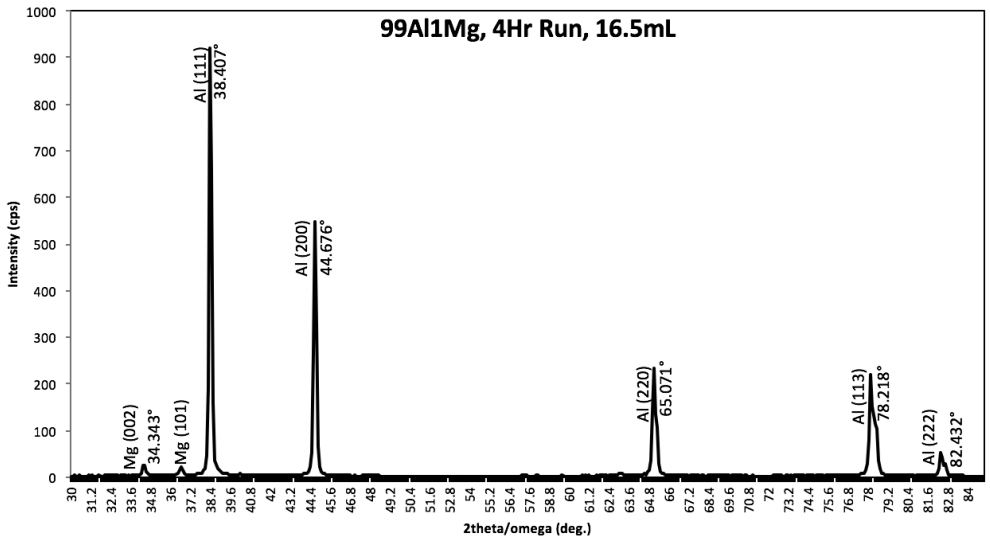

Figure 41: 99 atomic % aluminum, 1 atomic % magnesium milled for 4 hours with 2% SA and a 5:1 BPR. To produce a volume of approximately 16.5mL of powder, 21.373g of aluminum powder and 0.2g of magnesium powder. The resulting powder underwent XRD from 30°-85° with a count time (CT) of 30. Peaks that are present without an angle given to them are angles that Jade software did not pick up with either the Pearson VII or Pseudo-Voight approximations. The grain size was calculated to be 63.291nm and the strain was calculated to be 0.0003. Because there are still peaks of magnesium present, this system has not chemically mixed.

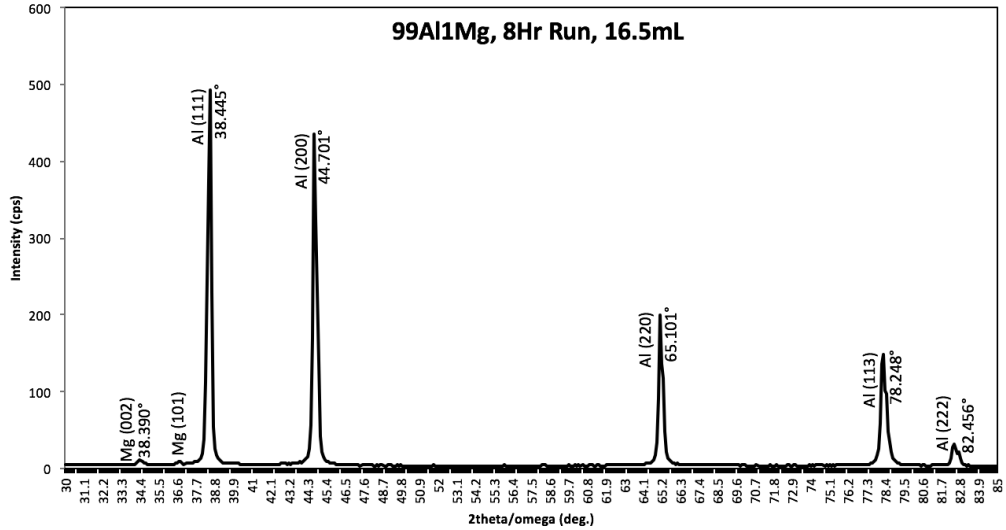

Figure 42: 99 atomic % aluminum, 1 atomic % magnesium milled for 8 hours with 2% SA and a 5:1 BPR. To produce a volume of approximately 16.5mL of powder, 21.4g of aluminum powder and 0.2g of magnesium powder. The resulting powder underwent XRD from 30°-85° with a count time (CT) of 75. Peaks that are present without an angle given to them are angles that Jade software did not pick up with either the Pearson VII or Pseudo-Voight approximations. The grain size was calculated to be 86.957nm and the strain was calculated to be 0.003. Because there are peaks of magnesium present, this system has not chemically mixed.

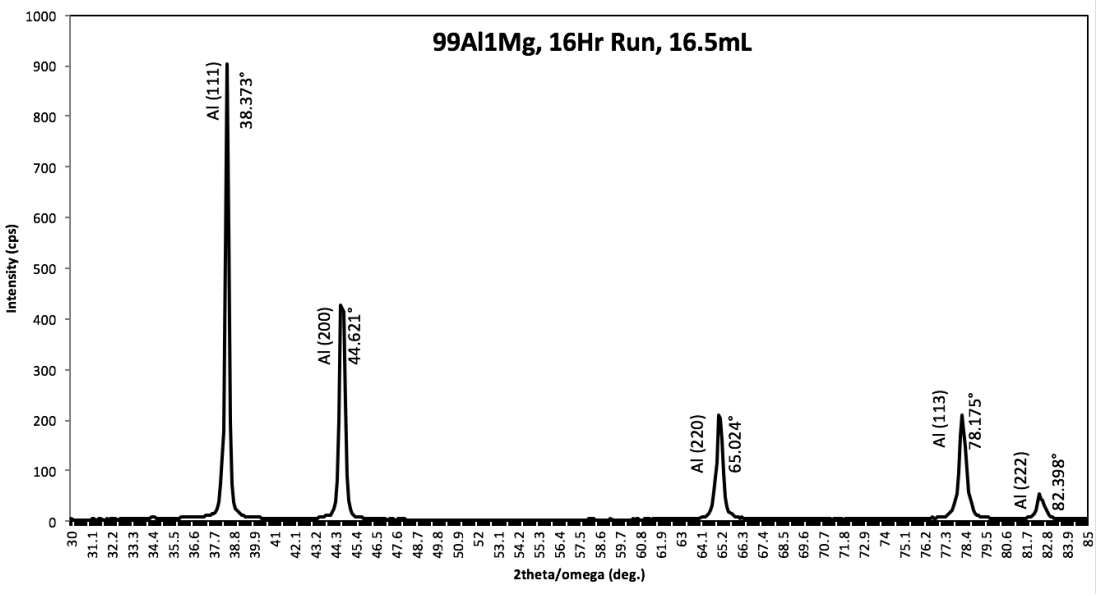

Figure 43: 99 atomic % aluminum, 1 atomic % magnesium milled for 16 hours with 2% SA and a 5:1 BPR. To produce a volume of approximately 16.5mL of powder, 21.576g of aluminum powder and 0.2g of magnesium powder. The resulting powder underwent XRD from 30°-85° with a count time (CT) of 90. Peaks that are present without an angle given to them are angles that Jade software did not pick up with either the Pearson VII or Pseudo-Voight approximations. The grain size was calculated to be 70.422nm and the strain was calculated to be 0.00095. Because there are no peaks of magnesium present, this system has chemically mixed.

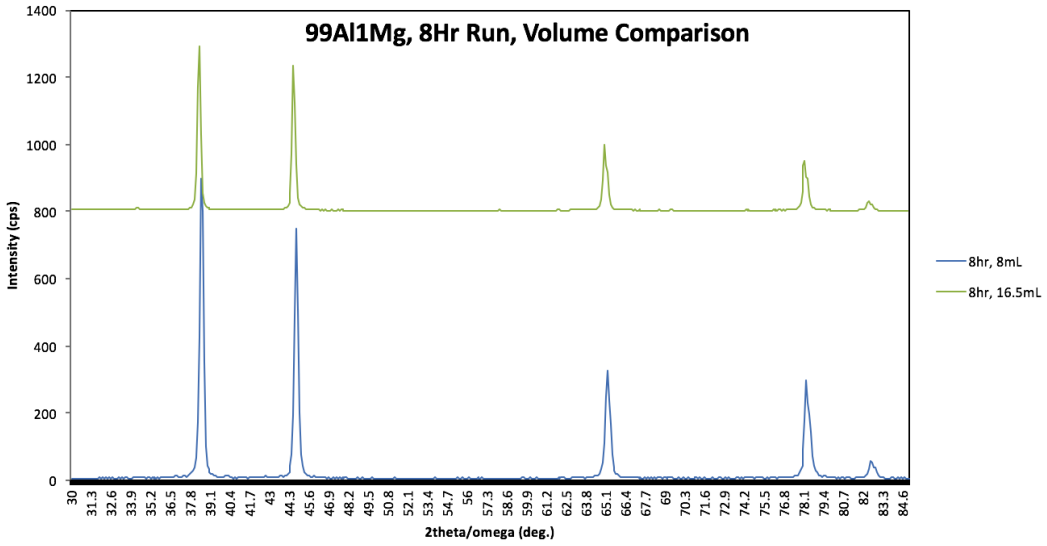

Figure 44: 99Al1Mg peaks after an 8Hr run with 8mL of powder and an 8Hr run with 16.5mL of powder. The 8Hr, 8mL run was able to chemically mix by the 8Hr mark. The 16.5mL run required more time to chemically mix because there was less free space available in the jar. Because there are still magnesium peaks present in the 16.5mL run and none for the 8mL run for the same milling time, there seems to be a dependence of chemical mixing upon free volume remaining in the jar.

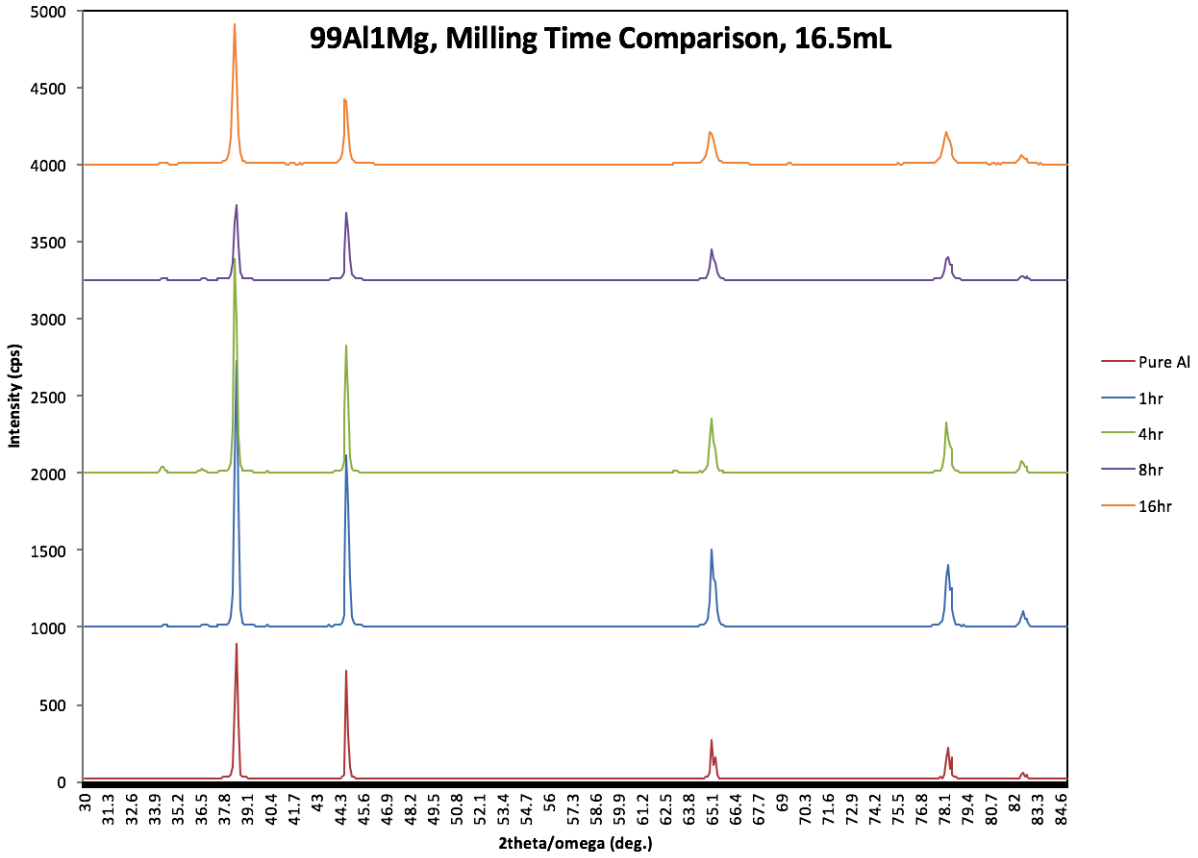

Figure 45: 99Al1Mg milling time comparison for 16.5mL runs. This run was able to chemically mix by the 16 hour mark. The magnesium peaks disappeared as the milling time increased, which proves that magnesium and aluminum did mix, like Murdoch and Schuh's thermodynamic model had suggested and S.M. Umbraikar et al. experimentally had proven [10,11]. There is a reduction in the magnesium peak over time, so this system can chemically mix over milling time.

3.4. Aluminum – Zirconium Alloys

99 atomic % aluminum and 1 atomic % zirconium were milled for 1 hour, 4 hours, 8 hours, and 16 hours at a powder volume of 16.5mL, and for 8 hours at a powder volume of 8mL. Because zirconium has a higher hardness than aluminum – 5MPa versus 2.75MPa – zirconium is not expected to chemically mix with aluminum; however, this powder system did mix during the 4Hr, 16.5mL run.

Results from these powder runs can be seen in Figure 46 through Figure 52.

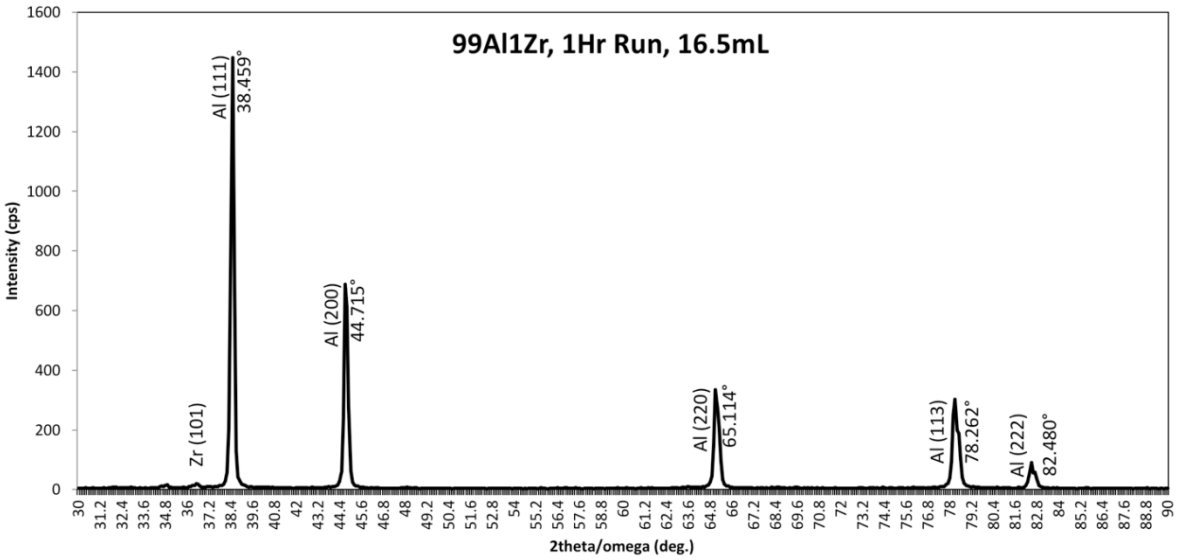

Figure 46: 99 atomic % aluminum, 1 atomic % zirconium milled for 1 hour with 2% SA and a 5:1 BPR. To produce a volume of approximately 16.5mL of powder, 20.88g of aluminum powder and 0.7g of silicon powder. The resulting powder underwent XRD from 30°-90° with a count time (CT) of 11. Peaks that are present without an angle given to them are angles that Jade software did not pick up with either the Pearson VII or Pseudo-Voight approximations. The grain size was calculated to be 57.471nm and the strain was calculated to be 0.0002. Because there are still peaks of zirconium present, this system has not chemically mixed.

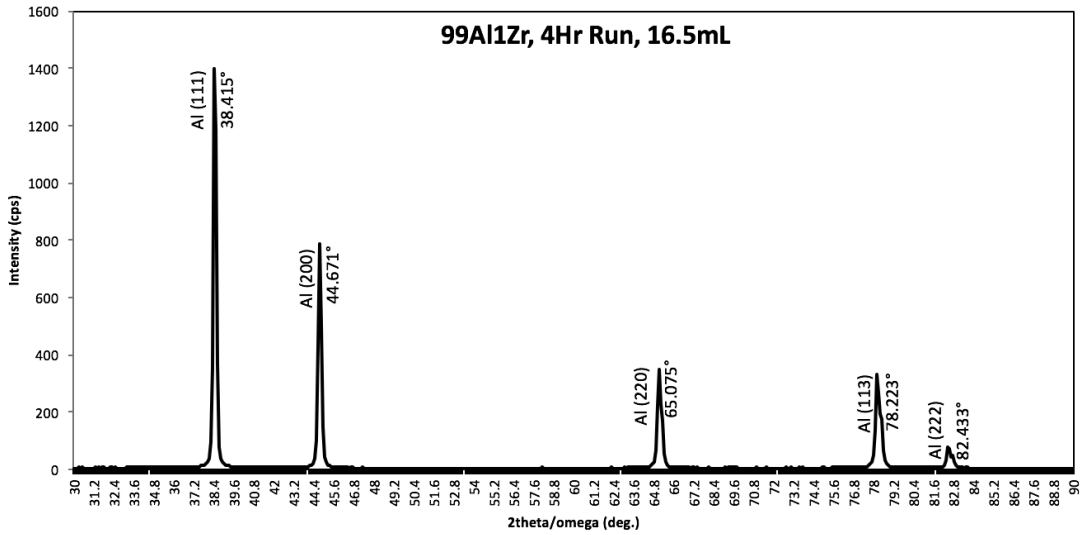

Figure 47: 99 atomic % aluminum, 1 atomic % zirconium milled for 4 hours with 2% SA and a 5:1 BPR. To produce a volume of approximately 16.5mL of powder, 20.871g of aluminum powder and 0.7g of silicon powder. The resulting powder underwent XRD from 30°-90° with a count time (CT) of 72. Peaks that are present without an angle given to them are angles that Jade software did not pick up with either the Pearson VII or Pseudo-Voight approximations. The grain size was calculated to be 59.880nm and the strain was calculated to be 0.0001. Because there are peaks of zirconium still present, this system has not chemically mixed.

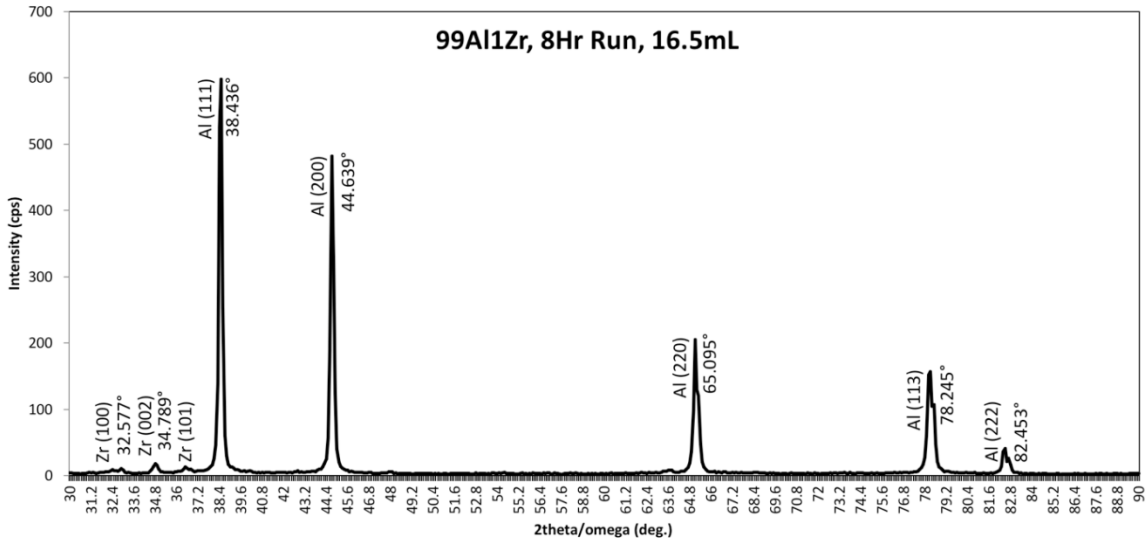

Figure 48: 99 atomic % aluminum, 1 atomic % zirconium milled for 8 hours with 2% SA and a 5:1 BPR. To produce a volume of approximately 16.5mL of powder, 20.885g of aluminum powder and 0.7g of silicon powder. The resulting powder underwent XRD from 30°-90° with a count time (CT) of 20. Peaks that are present without an angle given to them are angles that Jade software did not pick up with either the Pearson VII or Pseudo-Voight approximations. The grain size was calculated to be 13.774nm and the strain was calculated to be 0.00375. Because there are peaks of zirconium still present, this system has not chemically mixed.

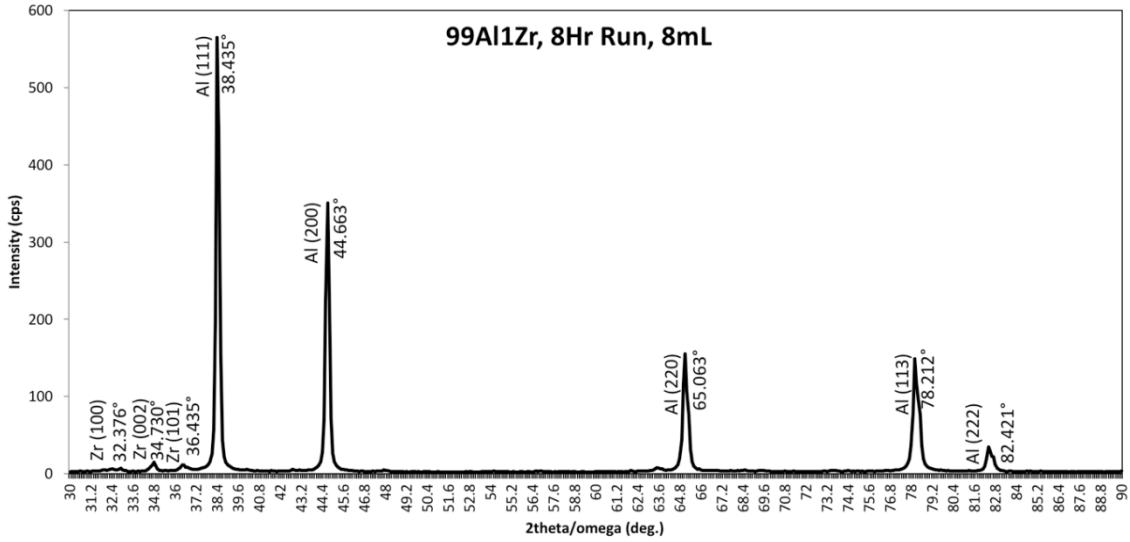

Figure 49: 99 atomic % aluminum, 1 atomic % zirconium milled for 8 hours with 2% SA and a 5:1 BPR. To produce a volume of approximately 8mL of powder, 10.138g of aluminum powder and 0.3g of silicon powder. The resulting powder underwent XRD from 30°-90° with a count time (CT) of 85. Peaks that are present without an angle given to them are angles that Jade software did not pick up with either the Pearson VII or Pseudo-Voight approximations. The grain size was calculated to be 0.112nm and the strain was calculated to be 1.0714. Because there are peaks of zirconium still present, this system has not chemically mixed.

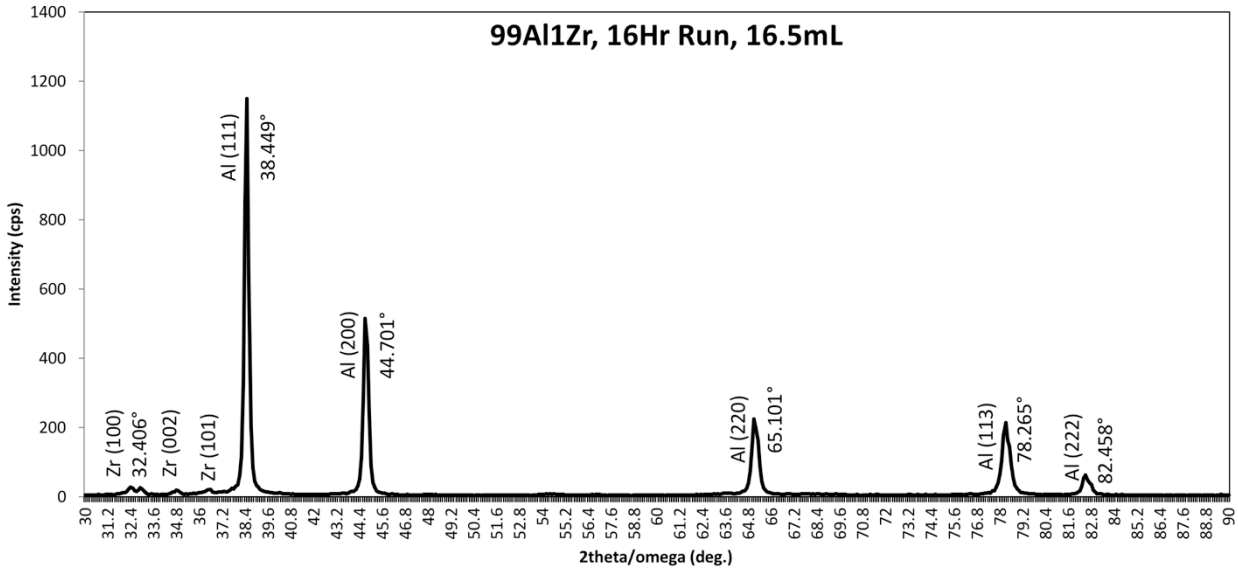

Figure 50: 99 atomic % aluminum, 1 atomic % zirconium milled for 16 hours with 2% SA and a 5:1 BPR. To produce a volume of approximately 16.5mL of powder, 20.87g of aluminum powder and 0.7g of silicon powder. The resulting powder underwent XRD from 30°-90° with a count time (CT) of 18. Peaks that are present without an angle given to them are angles that Jade software did not pick up with either the Pearson VII or Pseudo-Voight approximations. The grain size was calculated to be 31.447nm and the strain was calculated to be 0.00035. Because there are still peaks of zirconium present, this system has not chemically mixed.

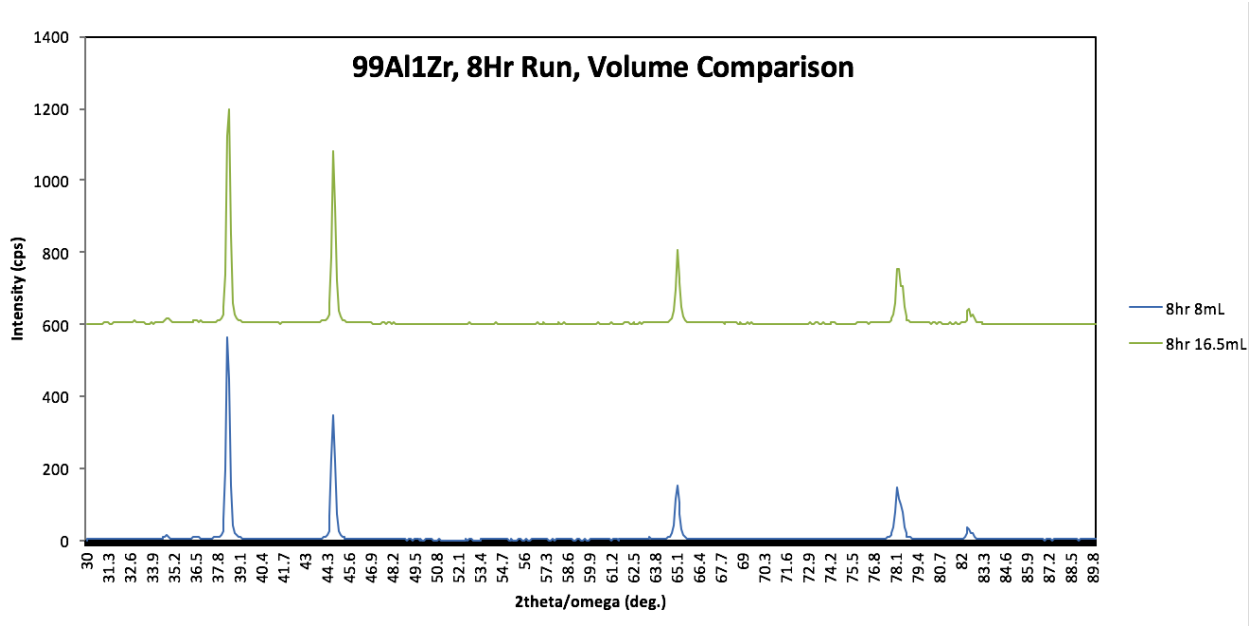

Figure 51: 99Al1Zr peaks after an 8Hr run with 8mL of powder and an 8Hr run with 16.5mL of powder. The difference in peak width is minimal; however, the 8mL run had the smaller grain size and had less strain. Increasing the empty jar volume did not encourage chemical mixing like in the aluminum – magnesium system.

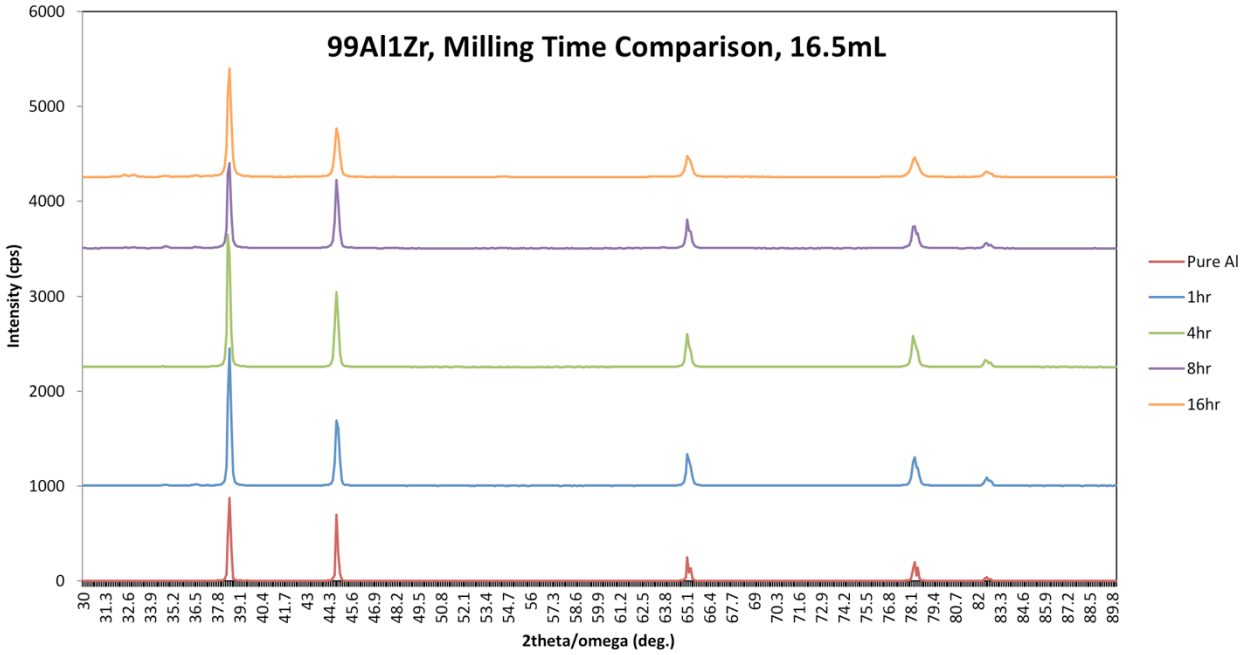

Figure 52: 99Al1Zr milling time comparison for 16.5mL runs. The Zn peaks became more defined as the milling time increased, which is interesting because zinc's hardness is slightly less than aluminum's – 2.5MPa versus 2.75MPa – the likelihood of this powder system chemically mixing compared to the aluminum-silicon system is greater. There seems be an increase in the zirconium peak over milling time, so the likelihood of this system chemically mixing seems very unlikely with increased milling time.

3.5. Synthesis of Results

Within this thesis work, aluminum – silicon alloys, aluminum – zinc alloys, aluminum – magnesium alloys, and aluminum – zirconium alloys were ball milled with a Retsch Planetary Ball Mill under an argon atmosphere. The samples were analyzed with a Rigaku Ultima III X-ray Diffractometer to determine whether or not these powder systems have chemically mixed. It was found that the 99Al1Mg powder system chemically mixed during the 8Hr, 8mL run and during the 16Hr, 16.5mL run, and the 99Al1Zr powder system chemically mixed during the 4Hr, 16.5mL run. The results obtained during this work somewhat matched the hypothesis that the likelihood of chemical mixing is dependent upon the mechanical properties (hardness) and

relative volume fraction of the harder element within the softer element, which are listed within Table 5.

Table 5: Comparison of Moh's Hardness values and crystal structures of aluminum and the secondary elements/solutes used [14].

Element:	Moh's Hardness (MPA):	Crystal Structure:
Al	2.75	Face Centered Cubic
Mg	2.5	Simple Hexagonal
Si	6.5	Tetrahedral Packing
Zn	2.5	Simple Hexagonal
Zr	5	Simple Hexagonal

In order for two elements to chemically mix, it was suggested that as long as both systems were mechanically similar and have similar structural properties. Some powder systems remain dual phase because plastic deformation occurs more likely within the softer phase material, and accordingly, the atoms do not shear across the interphase interface [54-56]. To encourage this "co-deformation," it has been suggested that milling elements with similar mechanical properties is one way to do this – as long as microstructure (crystal geometries), low volume fractions of hard elements, and mechanical properties (such as hardness) are considered when choosing elements to alloy during high energy mechanical alloying, then the results should be favorable [54,57-59]. Although these suggestions on ways to ensure chemical mixing occurs intuitively makes sense, the results achieved in this work do not prove that considering microstructure and mechanical properties alone leads to ideal chemical mixing scenarios. It is important to note that the difference in the obtained results versus the work of others can be due to incorrect high energy ball milling parameters, which will be discussed. Additionally, the

segregation enthalpies and mixing enthalpies with respect to stable binary nanocrystalline structures will be discussed and compared to the results obtained because mechanical properties and structure do not explain the results obtained within this work.

Despite the fact that magnesium and zinc have the same hardness value and the same crystal structure, as seen in Table 5, aluminum and magnesium chemically mixed and aluminum and zinc did not – which contradicts the idea of mechanical properties and structure can dictate ideal chemical mixing scenarios. Both magnesium and zinc have a Moh's hardness value of less than that of aluminum and both magnesium and zinc have a simple hexagonal structure – which perhaps, for reasons outside of mechanical properties and structure, enabled magnesium to easily be dissolved and chemically mix with the face-centered cubic structure of aluminum.

The aluminum-silicon system and the aluminum-zirconium system, due to secondary element's high hardness values compared to that of aluminum's hardness value, were expected to not mix at all if mechanical properties and structure of the alloying elements were considered; however, the 4Hr, 16.5mL aluminum-zirconium system did mix, which is an interesting and unexpected result. This interesting result may have occurred for various reasons. With the zirconium powders in particular, unlike the other powder systems, there seemed to be a lot of pre-defined tracks of the media and a lot of cold welding of the powders themselves. This means that there either is not enough free space within the jar and/or for this powder system, the wrong amount of process control agent was used (there might have been too little due to the large amount of cold welding which occurred) and/or the wrong process control agent was used. The solution ultimately would be to try to reduce the amount of free space in the jar, possibly increase the ball-to-powder ratio of this system, and/or increase the amount of process control agent. Additionally, to ensure that the motion of the grinding media is randomized, combining

smaller and larger media sizes is necessary, especially since this powder system displayed pre-defined tracks of motion [27]. Using the same sized grinding media (regardless of jar type) has been shown to produce tracks [17]. It is more ideal to have the media hit surfaces randomly than it is to have them traveling along a well-defined trajectory. Unideal ball milling parameters could be the reason why the 4Hr, 16.5mL run of the aluminum – zirconium alloy system was the only run to chemically mix, while the other runs did not achieve chemical mixing.

Besides the aluminum – magnesium alloy system, which was both theoretically and experimentally proven to chemically mix, the only other system within this work which produced results which aligned with the hypothesis about relative hardnesses/mechanical properties impacting the likelihood of chemical mixing was the aluminum – silicon alloy system. It did not matter if the milling time and/or the empty jar volume was changed, this system did not mix, which makes sense because it is hard to dissolve a very hard element into a very soft element through high energy ball milling.

Perhaps a reason why the results obtained during this work did not correlate to other experimental work/theoretical work which relates mechanical properties and microstructure to chemical mixing was because in this case, each powder system and each run did not plastically strain similarly, as shown in Figure 53. Z.C. Cordero and C.A. Schuh published an experimental and simulation paper to begin to understand the roles of the mechanical properties and microstructure of each elemental phase's role in mechanical alloying [54]. They milled W, $W_{50}Cr_{50}$, and $W_{50}Zr_{50}$ in a SPEX ball mill, in a steel vial, in an inert argon atmosphere, and a ball-to-powder ratio of 5:1 (same BPR as chosen for this work) [54]. Approximately 0.2g of powder was removed periodically for characterization purposes [54]. They calculated grain size of the powder post XRD with the Williamson-Hall method, like this work, and plotted data

points of each calculated grain size along with an exponential refinement trend common with grain sizes in milled powders, given by:

$$D = D_F + (D_O - D_F)e^{-k_l t} \quad [54]$$

where D_O is the initial grain size, D_F is the final grain size, t is the total milling time up till that point, k_l is a rate constant which is dependent upon material properties and milling parameters. The raw data they calculated using Williamson-Hall fit the exponential refinement trend as seen in Figure 53. In Figure 53, one can see the reduction in grain size at a very similar rate for all three powders. Because grain size is inversely proportional to the plastic strain that has been accumulated over time during the very early stages of ball milling, Figure 53 proves that W and Zr and W and Cr were deforming at the same rate because they were plastically strained similarly [54,63-64]. Data points with lines connecting each point for clarity of this work's calculated grain sizes using the Williamson-Hall method can be seen in Figure 54(a), the calculated exponential refinement trend for this work's data can be viewed in Figure 54(b) for clarity purposes.

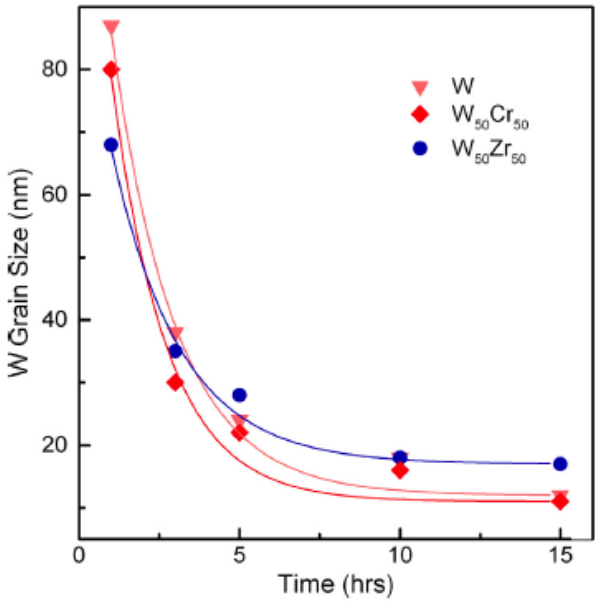

Figure 53: Grain size versus milling time, calculated with the Williamson-Hall method and shown as points, and an exponential refinement trend common to powders undergoing MA given by the equation above [54]. Because the grain refinement process was similar in all three powders, it is proof that they are plastically strained similarly, and therefore co-deform similarly [54].

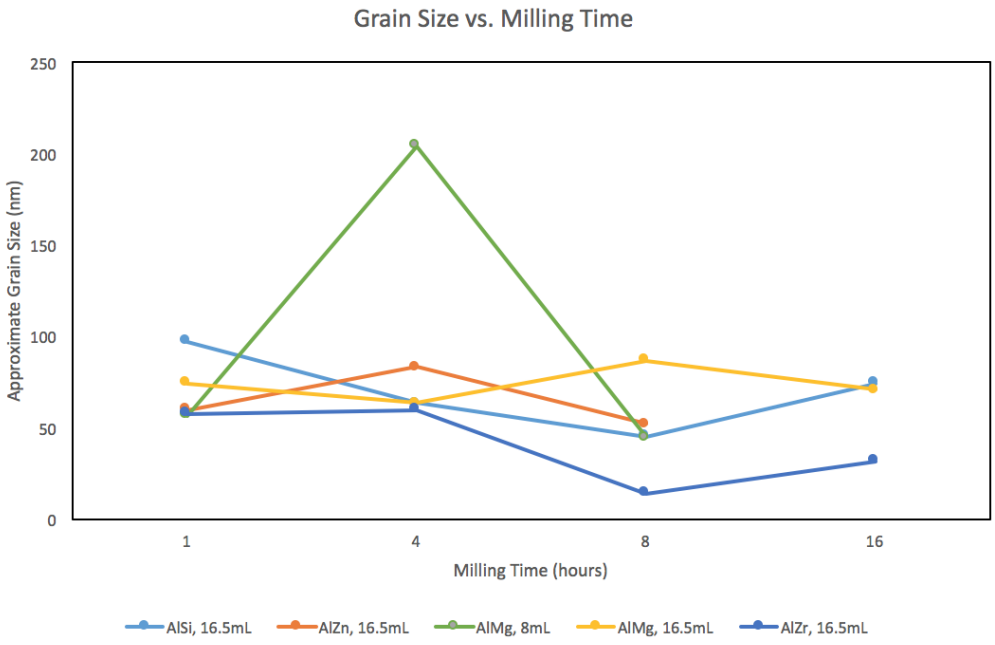

Figure 54(a): Grain size versus milling time calculated with the Williamson-Hall Method for AlSi, AlMg, AlZr, and AlZn. The decrease in grain size did not fit the exponential refinement trend seen in Figure 54(b), meaning that these powder systems did not co-deform at similar rates.

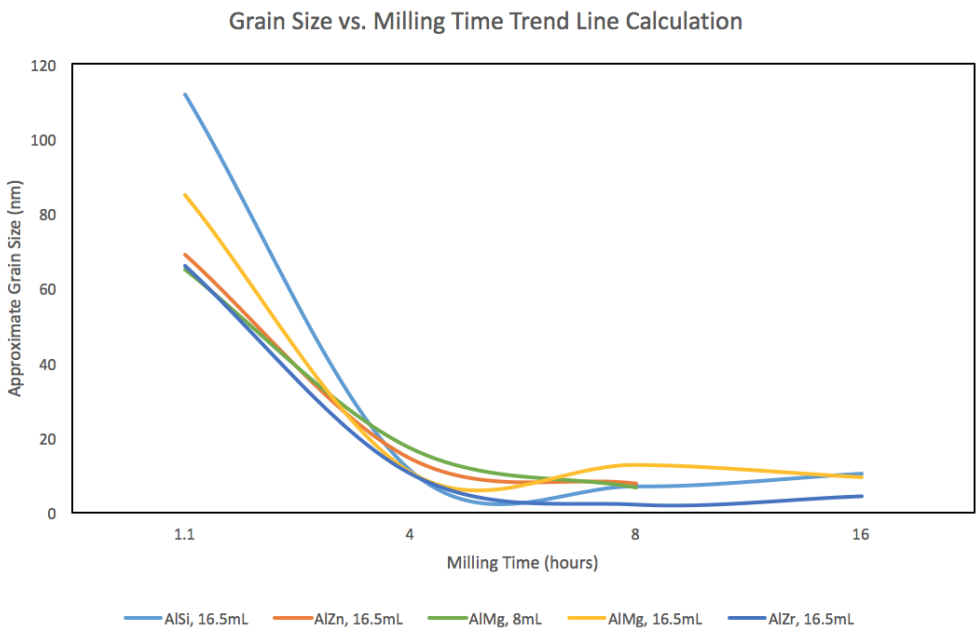

Figure 54(b): Calculated grain size exponential refinement trend for AlSi, AlZn, AlMg, and AlZr with the relationship $D = D_F + (D_O + D_F)e^{-klt}$. The calculated grain sizes in Figure 54(b) do not align with the typical exponential refinement trend common for most mechanically alloyed powders.

The k_l value was estimated in order to get the exponential refinement trend on a similar scale to that of the approximate grain size values in Figure 54(a). One can see that the calculated Williamson-Hall grain sizes did not fit the exponential refinement trend as it did in Figure 53. This can be because in the experiment done by Cordero and Schuh, they took approximately 0.2g of powder out periodically for characterization purposes (decreasing the variability in this trend line/data calculations in particular) unlike this experiment. From Figures 54(a) and (b), it is evident that the rate at which grain size decreased did not align with the exponential refinement trend, meaning in all powder systems and runs, the aluminum did not plastically strain similarly to each secondary elemental powder used, meaning co-deformation did not occur. However, in the aluminum-magnesium powder system, for both the 8mL volume runs and the 16.5mL runs, where chemical mixing did in fact occur, the rates of co-deformation between aluminum and

magnesium should have been similar according most theory which give mechanical properties and microstructure credit for co-deformation in mechanical alloying which leads to chemical mixing, disproving this mechanism to being valid, at least for these powder systems. Even if 0.2g of powder was not taken out periodically during each powder run for characterization (this data was compiled from many runs, not just one), the plastic straining experienced during each run be nearly similar, yielding results closer to that obtained in Cordero and Schuh if co-deformation occurred in the powder systems. Ideal mechanical properties and microstructure can lead to co-deformation, which increases the likelihood of chemical mixing; however, this is not the only mechanism by which chemical mixing occurs, as shown in the data obtained by this work.

The next steps in this analysis involve implementing the thermodynamic model proposed by Murdoch and Schuh by determining the enthalpy of dissolving of each aluminum-zinc system, comparing those values to the aluminum-magnesium system, and seeing if there is a difference which is significant enough to justify the results obtained experimentally [10]. Clearly, the mechanical and structural properties of powders cannot predict the likelihood of chemical mixing after all, there are more factors to consider. Additionally, it is important to mention that the results achieved by the magnesium-aluminum powder system were very similar to that achieved by another study, which is ideal [11].

There have been recent molecular dynamic studies which investigate an alloy's mechanical properties and how they impact the mechanism by which deformation/chemical mixing occurs, but despite this, there still is not a quantitative method to predict the mixibility of alloying systems [54-55,60-62]. Another approach to determining the enthalpy of segregation of these binary systems. The value of the enthalpy of segregation, in terms of binary systems, gives

the degree to which a solute will dissolve into the solvent's grain boundaries. A thermodynamic model proposed by H.A. Murdoch for the enthalpy of segregation for several binary systems can be seen in Figure 55. Unlike other thermodynamic models for binary systems, it incorporates grain boundary segregation [10]. The enthalpy of segregation can be described by the following:

$$\Delta H_0^{seg} = \zeta \left[\omega_c - \frac{\omega_{gb}}{2} - \frac{\Omega_{B\gamma B} - \Omega_{A\gamma A}}{2\zeta t} \right] \quad [10]$$

Where ω_c is the bulk crystalline interaction parameter (which is proportional to the enthalpy of mixing), γ_A and γ_B are the pure interfacial energies, Ω are the volume fractions, ς is the coordination number, and t is the grain boundary thickness [10].

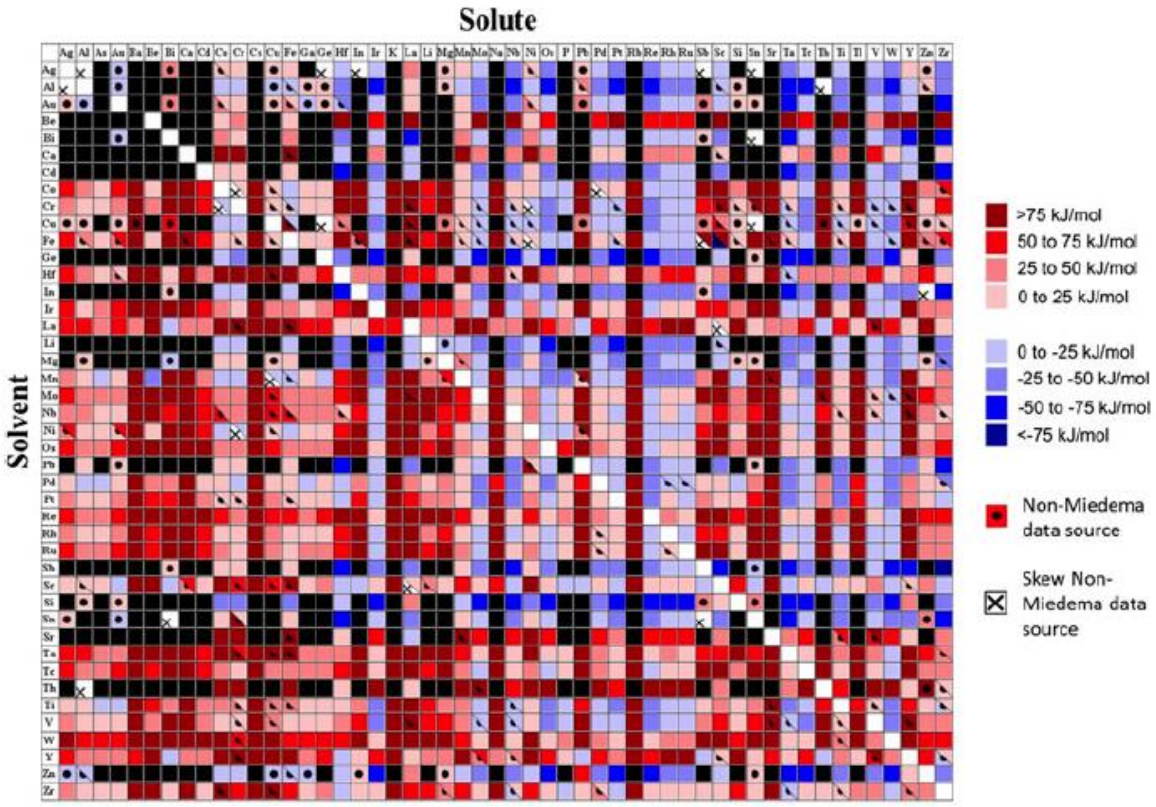

Figure 55: Calculated segregation enthalpies for binary systems using a thermodynamic model proposed by H.A. Murdoch and C.A. Schuh [10]. The value of the enthalpy of segregation for AlZr is -25 to -50kJ/mol, AlZn is 0 to 25kJ/mol, AlSi is 0 to 25kJ/mol, and AlMg is 0 to 25kJ/mol [10].

In Figure 55, the value of the enthalpy of segregation for AlZr is -25 to -50kJ/mol, AlZn is 0 to 25kJ/mol, AlSi is 0 to 25kJ/mol, and AlMg is 0 to 25kJ/mol [10]. In H.A. Murdoch's thesis work, the calculated values of the enthalpy of segregation of aluminum – magnesium was 12.7kJ/mol, aluminum – silicon was 5.3kJ/mol, aluminum – zinc was 7.1kJ/mol, and aluminum – zirconium was -49.5kJ/mol [65]. The results do in fact correlate with what was obtained experimentally! The two powder systems which experienced chemical mixing have the highest values of enthalpy of segregation, meaning the solute atoms must be able to segregate themselves within the surface or interface of the solute in order to minimize the overall free energy of the binary system. Aluminum – magnesium has the highest positive enthalpy of segregation, meaning that it is likely to chemically mix in order to reduce the overall free energy of the system, and that magnesium will wind up in the grain boundaries of the aluminum. Aluminum-zirconium has the highest negative enthalpy of segregation, meaning it will chemically mix in order to reduce the free energy of the system; however, zirconium will not wind up in the grain boundaries of the aluminum. Aluminum – silicon and aluminum – zinc have low enough enthalpies of segregation where it was not needed to chemically mix in order to reduce the amount of free energy in the system.

In addition to understanding the reasoning behind how chemical mixing occurs in mechanically alloyed powder systems, there was an interesting result which needs to be mentioned. In the aluminum-magnesium alloy system, a powder volume of eight milliliters (meaning that approximately greater than or equal to fifty percent of the jar volume was empty) achieved a chemically mixed state within eight hours, while a powder volume of sixteen and a half milliliters (meaning that approximately one-third of the jar volume was empty) could not achieve a chemically mixed state within eight hours, but it eventually did within sixteen hours of

milling time. This suggests that there is an empty space jar volume dependence upon the rate at which a powder system chemically mixes, which can be a strong dependence to consider, especially for trying to create models which either predict ideal ball milling parameters and/or are used to determine whether or not powder systems do mix. Further testing with other powder systems that do chemically mix need to be tested to prove this result.

Chapter 4: Concluding Remarks and Future Work

Within this thesis work, 99 atomic % aluminum 1 atomic % silicon, 99 atomic % aluminum 1 atomic % zinc, 99 atomic % aluminum 1 atomic % magnesium, and 99 atomic % aluminum 1 atomic % zirconium were ball milled with a Retsch Planetary Ball Mill under an argon atmosphere. The samples were then analyzed with a Rigaku Ultima III X-ray Diffractometer to determine whether or not these powder systems have chemically mixed. It was found that the 99Al1Mg powder system chemically mixed during the 8Hr, 8mL run and during the 16Hr, 16.5mL run, and the 99Al1Zr powder system chemically mixed during the 4Hr, 16.5mL run.

Despite the fact that magnesium and zinc had the same hardness, magnesium and aluminum chemically mixed and zinc did not. Both magnesium and zinc have a simple hexagonal structure, so perhaps the next steps in this analysis involve implementing the thermodynamic model proposed by Murdoch and Schuh by determining the enthalpy of mixing and the enthalpy of dissolving of the aluminum-zinc system, comparing those values to the aluminum-magnesium system, and seeing if there is a difference which is significant enough to justify the results obtained experimentally [10]. Additionally, the results achieved by the

magnesium-aluminum powder system were very similar to that achieved by another study, which is ideal [11].

Interestingly, in the aluminum-magnesium section, a powder volume of 8mL (meaning that approximately greater than or equal to fifty percent of the jar volume was empty) achieved a chemically mixed state within eight hours, while a powder volume of 16.5mL (meaning that approximately one-third of the jar volume was empty) could not achieve a chemically mixed state within eight hours, but it eventually did within sixteen hours. This suggests that there is an empty space jar volume dependence upon the rate at which a powder system chemically mixes, which can be a strong dependence to consider, especially for trying to create models which either predict ideal ball milling parameters and/or are used to determine whether or not powder systems do mix. Further testing with other powder systems that do chemically mix need to be tested to prove this result.

The aluminum-silicon system and the aluminum-zirconium system, due to secondary element's high hardness values compared to that of aluminum's hardness value, were expected to not mix at all, however, the 4Hr, 16.5mL aluminum-zirconium system did mix, which is an interesting result. This interesting result may have occurred for various reasons. With the zirconium powders in particular, unlike the other powder systems, there seemed to be a lot of pre-defined tracks of the media and a lot of cold welding of the powders themselves. This means that there either is not enough free space within the jar and/or for this powder system, the wrong amount of process control agent was used (there might have been too little due to the large amount of cold welding which occurred) and/or the wrong process control agent was used. The solution ultimately would be to try to reduce the amount of free space in the jar, possibly increase the ball-to-powder ratio of this system, and/or increase the amount of process control

agent. Additionally, to ensure that the motion of the grinding media is randomized, combining smaller and larger media sizes is necessary, especially since this powder system displayed pre-defined tracks of motion [27]. Using the same sized grinding media (regardless of jar type) has been shown to produce tracks [17]. It is more ideal to have the media hit surfaces randomly than it is to have them traveling along a well-defined trajectory.

The reasoning behind the results that were obtained in this thesis work was not due to the mechanical properties and microstructure of the binary powder system, it was in fact because of the enthalpy of segregation of the binary, aluminum powder systems which influenced the degree of mixing. In H.A. Murdoch's thesis work, the calculated values of the enthalpy of segregation of aluminum – magnesium was 12.7kJ/mol, aluminum – silicon was 5.3kJ/mol, aluminum – zinc was 7.1kJ/mol, and aluminum – zirconium was -49.5kJ/mol [65]. The results do in fact correlate with what was obtained experimentally! The two powder systems which experienced chemical mixing have the highest values of enthalpy of segregation, meaning the solute atoms must be able to segregate themselves within the surface or interface of the solute in order to minimize the overall free energy of the binary system. Aluminum – magnesium has the highest positive enthalpy of segregation, meaning that it is likely to chemically mix in order to reduce the overall free energy of the system, and that magnesium will wind up in the grain boundaries of the aluminum. Aluminum-zirconium has the highest negative enthalpy of segregation, meaning it will chemically mix in order to reduce the free energy of the system; however, zirconium will not wind up in the grain boundaries of the aluminum. Aluminum – silicon and aluminum – zinc have low enough enthalpies of segregation where it was not needed to chemically mix in order to reduce the amount of free energy in the system.

In order to continue this work, there are some things that could be done in the future. One, being, to further prove the free jar volume dependence on the rate of chemical mixing of a powder system with other powder systems that have the potential to chemically mix. In addition, Transmission Electron Microscopy and annealing should be performed in future. Occasionally, it might be necessary to anneal mechanically alloyed powders in order to further encourage chemical mixing. In the case of the aluminum zirconium system, there may be more runs undergoing chemical mixing post an annealing process [17]. After the annealing process, XRD should be performed and then compared to the unannealed samples to see if chemical mixing was encouraged due to annealing process. Additionally, in order to ensure that the secondary powder did *in fact* dissolve into the primary powder's grain boundaries, Transmission Electron Microscopy must be performed. Although, XRD can provide enough contrast in data to possibly prove chemical mixing occurred, XRD cannot accurately determine solid solubility limits [17].

References:

[1] K.S. Kumar, H. Van Swygenhoven, S. Suresh, Acta Mater. 51 (2003) 5743-5774.

[2] H.A. Padilla, B.L. Boyce, Exp. Mech. 50 (2010) 5 -23.

[3] D.H. Jeong, F. Gonzalez, G. Palumbo, K.T. Aust, U. Erb, Scr. Mater. 44 (2001) 493-499.

[4] H. Gleiter, Prog. Mater. Sci 33 (1989) 223-315.

[5] J.R. Weertman, Mechanical Behavior of Nanocrystalline Metals, in: C.C. Kosh (Eds.), Nanostructured Materials – Processing, Properties, and Applications, William Andrew, NY, 2001, p. 537-565.

[6] A.R. Kalidindi, T. Chookajorn, C.A. Schuh, The Minerals, Metals, & Materials Society, 67 (2015) 2834-2843.

[7] J.W. Cahn, Acta Metall. 10 (1962) 789.

[8] T. Chookajorn, H.A. Murdoch, and C.A. Schuh, Science, 337 (2012) 951.

[9] G.J. Tucker, D.L. McDowell, Inter. J. Plast. 27 (2011) 841-857.

[10] H.A. Murdoch, C.A. Schuh, J. Mater. Res. 28 (2013) 2154-2163.

[11] S.M. Umbrajkar, M. Schoenitz, S.R. Jones, E.L. Dreizin, Journal of Alloys and Compounds 402 (2005) 70-77.

[12] Z.C. Cordero, C.A. Schuh, Acta Materialia 82 (2014) 123-136.

[13] C.W. Sinclair, J.D. Embury, G.C. Weatherly, Mater. Sci. Eng. A 272 (1999) 90-98.

[14] in: P.P. Table (Ed.), periodictable.com.

[15] W.D. Callister, in: J. Hayton (Ed.), John Wiley & Sons, Inc. , New York, NY, 2007.

[16] X. Sauvage, F. Wetscher, P. Pareige, Acta Materialia, 53 (2005) 2127-2135.

[17] C. Suryanarayana, Progress in Materials Science, 46 (2001) 1-184.

[18] C. Suryanarayana, E. Ivanov, V.V. Boldyrev, Materials Science and Engineering A 304-306 (2001) 151-158.

[19] J.L. Harringa, B.A. Cook, B.J. Beaudry, Journal of Materials Science 27 (1992) 801-804.

[20] Watanabe R, Hashimoto H, Park Y-H. In: Pease III LF, Sansoucy RJ, editors. Advances in powder metallurgy 1991, vol. 6. Princeton, NJ: Metal Powder Industries Federation, 1991. p.119-30.

[21] Park Y-H, Hashimoto H, Watanabe R. Mater Sci Forum 1992;88-90:59-66.

[22] Guo W, Iasonna A, Magini M, Martelli S, Padella F. J Mater Sci 1994;29:2436-44.

[23] Padella F, Paradiso E, Burgio N, Magini M, Martelli S, Guo W, Iasonna A. J Less-Common Metals 1991;175:79±90.

[24] Gilman PS, Benjamin JS. Annu Rev Mater Sci 1983;13:279-300.

[25] Gavrilov D, Vinogradov O, Shaw WJD. In: Poursartip A, Street K, editors. Proc. Inter. Conf. on Composite Materials, ICCM-10, vol. III. Woodhead Publishing, 1995, p. 11.

[26] Takacs L, Pardavi-Horvath M. J Appl Phys 1994;75:5864-6.

[27] Takacs L. In: Suryanarayana C, et al., editors. Processing and properties of nanocrystalline materials. Warrendale, PA: TMS, 1996. p. 453±64.

[28] C. Suryanarayana, G.H. Chen, F.H. Froes, Scripta Metall Mater 26 (1992) 1727-1732.

[29] Frazier WE, Koczak MJ. Scripta Metall 1987;21:129-34.

[30] Chen G, Wang K, Wang J, Jiang H, Quan M. In: deBarbadillo JJ, et al., editors. Mechanical alloying for structural applications. Materials Park, OH: ASM International, 1993. p. 183-7.

[31] Lai MO, Lu L. Mechanical alloying. Boston, MA: Kluwer Academic Publishers, 1998.

[32] Hong LB, Bansal C, Fultz B. Nanostructured Mater 1994;4:949-56.

[33] Qin Y, Chen L, Shen H. J Alloys and Compounds 1997;256:230-3.

[34] Kimura H, Kimura M. In: Clauer AH, deBarbadillo JJ, editors. Solid state powder processing. Warrendale, PA: TMS, 1990. p. 365-77.

[35] Yamada K, Koch CC. J Mater Res 1993;8:1317-26.

[36] Koch CC, Pathak D, Yamada K. In: deBarbadillo JJ, et al., editors. Mechanical alloying for structural applications. Materials Park, OH: ASM International, 1993. p. 205-12.

[37] Benjamin JS. Sci Amer 1976;234(5):40-8.

[38] Benjamin JS, Volin TE. Metall Trans 1974;5:1929-34.

[39] Benjamin JS. Metal Powder Rep 1990;45:122-7.

[40] Lee PY, Koch CC. J Mater Sci 1988;23:2837-45.

[41] in: Retsch (Ed.) Milling Products, Retsch www.retsch.com.

[42] in: D.o.C.M. Physics (Ed.), P.J. Šafárik University Institute of Physics, exphys.science.upjs.sk

[43] Schulz R, Trudeau M, Huot JY, Van Neste A. Phys Rev Lett 1989;62:2849-52.

[44] Mikhailenko SD, Kalinina OT, Dyunusov AK, Fasman AB, Ivanov E, Golubkova GB. Siberian J Chem 1991;5:93-104.

[45] Customer Magazine, Retsch, pp. 1-20.

[46] RETSCH Product Navigator, Retsch, ninlab.se, pp. 1-16.

[47] Dutrow BL, Clark CM. in: Science Education Resource Center at Carleton College (Ed.) Geochemical Instrumentation and Analysis, Carleton College, serc.carleton.edu, 2016.

[48] Poly Crystallography, Inc., polycrystallography.com.

[49] Thornton, Steven T. and Rex, Andrew, Modern Physics for Scientists and Engineers, Saunders College Publishing, 1993.

[50] in: G. Beaucage (Ed.), College of Engineering & Applied Science, University of Cincinnati

eng.uc.edu.

[51] S.A. Speakman, in: MIT Center for Materials Science and Engineering (Ed.), MIT, prism.mit.edu/xray.

[52] Barnes P, Jacques S, Vickers M, in: B.C. School of Crystallography, University of London (Ed.) Advanced Certificate in Powder Diffraction on the Web, School of Crystallography, Birkbeck College, University of London, pd.chem.ucl.ac.uk, 2006.

[53] Institute of Experimental Mineralogy Russian Academy of Sciences, database.iem.ac.ru.

[54] C.A.Shuh, Z.C. Cordero, Acta Materialia, 82 (2014) 123-136.

[55] Y.Ashkenazy, et al., Acta Materialia, 60 (2012) 984-993.

[56] F. Delogu, Journal of Applied Physics, 104 (2008).

[57] B.Fultz, L.B. Jong, Acta Materialia, 46 (1998) 2937-2946.

[58] J. Xu et al., Acta Materialia, 47 (1999) 1241-1253.

[59] M. Atzmon et al., Journal of Metastable and Nanocrystalline Materials, 10 (2001) 311-316.

[60] S.Odunuga et al., APS Physics, 95 (2005).

[61] N.O. Vo et al., Journal of Materials Research, 27 (2012) 1621 - 1630.

[62] N.Q.Vo et al., JOM, 65 (2013) 382-389.

[63] F. Delugo, JOM, 42 (2007) 4356-4363.

[64] F. Delogu, Materials Science & Engineering A, 422 (2006) 198-204.

[65] H.A. Murdoch, Materials Science and Engineering, Massachusetts Institute of Technology, 2013, pp. 216.